





FRET kinase sensor development reveals SnRK2/OST1 activation by ABA but not by MeJA and high CO₂ during stomatal closure

Li Zhang^{1†‡}, Yohei Takahashi^{1†*}, Po-Kai Hsu¹, Hannes Kollist², Ebe Merilo², Patrick J Krysan³, Julian I Schroeder^{1*}

¹Cell and Developmental Biology Section, Division of Biological Sciences, University of California, San Diego, San Diego, United States; ²Institute of Technology, University of Tartu, Tartu, Estonia; ³Horticulture Department, University of Wisconsin-Madison, Madison, United States

Abstract Sucrose-non-fermenting-1-related protein kinase-2s (SnRK2s) are critical for plant abiotic stress responses, including abscisic acid (ABA) signaling. Here, we develop a genetically encoded reporter for SnRK2 kinase activity. This sensor, named SNACS, shows an increase in the ratio of yellow to cyan fluorescence emission by OST1/SnRK2.6-mediated phosphorylation of a defined serine residue in SNACS. ABA rapidly increases FRET efficiency in *N. benthamiana* leaf cells and *Arabidopsis* guard cells. Interestingly, protein kinase inhibition decreases FRET efficiency in guard cells, providing direct experimental evidence that basal SnRK2 activity prevails in guard cells. Moreover, in contrast to ABA, the stomatal closing stimuli, elevated CO₂ and MeJA, did not increase SNACS FRET ratios. These findings and gas exchange analyses of quintuple/sextuple ABA receptor mutants show that stomatal CO₂ signaling requires basal ABA and SnRK2 signaling, but not SnRK2 activation. A recent model that CO₂ signaling is mediated by PYL4/PYL5 ABA-receptors could not be supported here in two independent labs. We report a potent approach for real-time live-cell investigations of stress signaling.

*For correspondence: ytakahashi@UCSD.EDU (YT); jischroeder@ucsd.edu (JIS)

[†]These authors contributed equally to this work

Present address: [‡]Maize Research Institute, Sichuan Agricultural University, Wenjiang, China

Competing interests: The authors declare that no competing interests exist.

Funding: See page 22

Received: 25 February 2020 Accepted: 20 May 2020 Published: 28 May 2020

Reviewing editor: Dominique C Bergmann, Stanford University, United States

© Copyright Zhang et al. This article is distributed under the terms of the Creative Commons Attribution License, which permits unrestricted use and redistribution provided that the original author and source are credited.

Introduction

Protein phosphorylation of downstream substrates by protein kinases is a central and critical molecular switch for activation of many cell biological processes (Ardito et al., 2017; Stone and Walker, 1995). However, investigation of protein kinase activities remains a challenge, particularly real-time measurements in living cells. In-gel kinase assays are the most common method for measuring protein kinase activities using the (auto-)phosphorylation state of a kinase or a substrate as indicator of the kinase activity (Manning et al., 2002). With this method, it is difficult to track dynamic kinase activity in specific cell types or tissues, and time course measurements in living cells and subcellular analyses are not feasible (Aoki et al., 2012). To overcome this drawback, a first Förster resonance energy transfer (FRET) biosensor reporting the activity of cAMP-dependent protein kinase A (PKA) was developed by R.Y. Tsien and colleagues (Zhang et al., 2001). The design of a FRET-based protein kinase biosensor includes a phosphorylatable substrate protein domain and a phosphorylation recognition domain that together can drive a conformational change between two fluorophores (Sample et al., 2014; Ting et al., 2001; Wang et al., 2005; Gao and Zhang, 2008; Miyawaki and Tsien, 2000). In the presence of active protein kinase, the substrate domain is phosphorylated, which results in a high affinity to the phosphorylation-recognition domain. This enhanced affinity between the two domains can trigger the two fluorophores to be in closer proximity to one-another



(Jones et al., 2013). Such a conformational change can cause higher FRET efficiency (Lin et al., 2019; Jones et al., 2013). In plants, only one protein kinase FRET biosensor has been reported to date, that senses plant MAP kinase activity using a MAPK substrate domain (MAP kinase phosphatase, MKP1) and a FHA domain (Zaman et al., 2019).

Plants have to cope with diverse and complex abiotic and biotic stresses. Abscisic acid (ABA) is a plant hormone, which plays a central role in plant drought, cold and salinity stress tolerance (Cutler et al., 2010; Raghavendra et al., 2010; Zhu, 2016). SnRK2 protein kinases (sucrose non-fermenting-1-related protein kinase 2s) are members of a plant-specific serine/threonine kinase family that play critical roles in ABA signal transduction (Fujii et al., 2007; Mustilli et al., 2002; Yoshida et al., 2002; Fujii and Zhu, 2009). ABA activation of SnRK2 protein kinases has been found in several species including Vicia faba (Li et al., 2000), rice (Kobayashi et al., 2004), Arabidopsis (Hrabak et al., 2003; Fujii and Zhu, 2009), Glycine soja (Yang et al., 2012) and Triticum polonicum (Wang et al., 2015). In Arabidopsis, there are 10 SnRK2 family members (SnRK2.1-2.10) in the genome. Three of these protein kinases, SnRK2.2, SnRK2.3 and SnRK2.6/OST1, are strongly activated by ABA. The SnRK2.6/OST1 gene is expressed in stomatal guard cells (Mustilli et al., 2002). SnRK2.6/OST1 mediates reduction of stomatal apertures and plays a pivotal role in ABA-induced stomatal closure (Yoshida et al., 2002; Mustilli et al., 2002). In addition, SnRK2.6/OST1 is genetically required for rapid stomatal closure in response to elevation in the CO2 concentration (Xue et al., 2011; Merilo et al., 2013; Hsu et al., 2018). Furthermore, SnRK2.6/OST1 is also required for methyl jasmonate (MeJA)-induced stomatal closure (Yin et al., 2016). However, whether MeJA or CO₂ activate OST1/SnRK2.6 protein kinases in guard cells and whether CO₂ rapidly activates ABA signaling remains controversial.

Studies have shown Methyl jasmonate (MeJA)-induced stomatal closure in several species (Herde and Pena-Cortes, 1997; Gehring, 1997; Suhita et al., 2004; Akter et al., 2012; Förster et al., 2019) and that MeJA-induced stomatal closing is impaired in snrk2.6/ost1 mutants (Yin et al., 2016; Munemasa et al., 2019). Unexpectedly, however, recent in-gel kinase assays with isolated guard cell protoplasts detected no MeJA-induced enhancement of OST1 kinase activity (Munemasa et al., 2019).

Classical research demonstrated that ABA enhances CO₂-induced stomatal closing and vice versa (*Raschke, 1975*; *Raschke et al., 1976*). In addition, plants have previously been found to have higher basal ABA concentrations in guard cells than in leaf mesophyll cells (*Lahr and Raschke, 1988*). ost1 mutant alleles have been shown to impair CO₂-induced stomatal closing in intact leaves and intact plants (*Xue et al., 2011*; *Merilo et al., 2013*), but not as strongly as ABA-induced stomatal closing (*Hsu et al., 2018*). Unexpectedly, however, recent *in-gel* kinase assays show no CO₂ activation of SnRK2 kinases in purified guard cells protoplasts (*Hsu et al., 2018*). Moreover, whether ABA-SnRK2 signal transduction is directly activated by CO₂ elevation remains controversial (*Chater et al., 2015*; *Merilo et al., 2013*; *Hsu et al., 2018*; *Dittrich et al., 2019*). The requirement to use guard cell extracts for monitoring OST1/SnRK2.6 activity hampers resolution of this question that is key to understanding how the distinct stimuli CO₂, ABA and MeJA merge in mediation of stomatal closing.

In-gel kinase assay analyses have shown that ABA rapidly activates OST1/SnRK2.6/AAPK protein kinases using purified guard cell protoplasts (Li et al., 2000; Mustilli et al., 2002; Hsu et al., 2018; Li and Assmann, 1996; Mori and Muto, 1997). ABA-activated SnRK2 protein kinases phosphorylate several downstream substrates including the SLAC1 anion channel and transcription factors (Takahashi et al., 2013; Munemasa et al., 2019; Geiger et al., 2009; Furihata et al., 2006; Lee et al., 2009). ABA-responsive kinase substrate 1 (AKS1) is a basic helix-loop-helix (bHLH) transcription factor (Takahashi et al., 2013). AKS1 was demonstrated to be phosphorylated by SnRK2s in response to ABA in Arabidopsis guard cells, as an endogenous phosphorylation substrate (Takahashi et al., 2017; Takahashi et al., 2013). Moreover, ABA rapidly induces 14-3-3 protein binding to AKS1 in a phosphorylation-dependent manner in guard cells (Takahashi et al., 2013). 14-3-3 proteins are conserved proteins in eukaryotes and known for binding to target proteins upon phosphorylation. 14-3-3 proteins recognize two typical 14-3-3 binding motifs, which in AKS1 are the Ser-30 residue and Ser-157 residue (Takahashi et al., 2013). The AKS1 (S30A/S157A) mutant protein does not bind to the 14-3-3 protein GF14phi (Takahashi et al., 2013).

Here, using AKS1 and an Arabidopsis 14-3-3 protein, GF14phi, we describe the development of a genetically-encoded FRET-based biosensor, named <u>SnRK2 activity sensor</u> (SNACS), that reports



SnRK2 protein kinase activity in live plant cells in real-time. We observe real-time SnRK2 kinase activity in response to ABA in living plant cells. ABA-induced FRET shifts are disrupted in snrk2.2/2.3/ ost1 triple mutant guard cells. In addition, we also demonstrate the effects of protein kinase inhibitors on SNACS in planta, showing that SNACS FRET shifts are reversible and providing evidence that basal ABA signaling exists in guard cells. Moreover, using this sensor, we show that, in contrast to ABA, MeJA and CO2 do not cause SNACS FRET ratio increases in guard cells in real-time in vivo analyses. A model that is consistent with the presented findings in guard cells is discussed, in which basal ABA/SnRK2 signaling is required for CO₂ and MeJA responses, but without direct activation of SnRK2 kinases. In addition, gas exchange analyses with ABA receptor quintuple and sextuple mutants, performed independently in two of our laboratories (EM, HK and JIS), could not confirm a recent report that stomatal CO2 signaling is mediated by the PYL4 and PYL5 ABA-receptors (Dittrich et al., 2019). Imaging using SNACS enables resolution of single cell-type recordings, compared to the need to laboriously isolate and purify >10⁵ guard cell protoplasts from >100 leaves for each guard cell in-gel kinase assay lane. Taken together, a genetically-encoded FRET-based biosensor is developed that reports real-time basal and stimulus-dependent SnRK2 protein kinase activity in single plant cells.

Results

Construction of SnRK2 protein kinase activity sensor

In order to attempt production of a genetically encoded biosensor that would report SnRK2 kinase activity in *Arabidopsis*, we used a 48 amino acid domain surrounding the serine-30 residue of the *Arabidopsis* ABA-RESPONSIVE KINASE SUBSTRATE1 transcription factor (AKS1, At1g51140) (*Takahashi et al., 2013*). Furthermore, an AKS1 binding domain was inserted into the construct encoding the *Arabidopsis* full length 14-3-3 protein, GF14phi (267 amino acids). AKS1 has been shown to be phosphorylated by SnRK2s at the serine-30 residue (*Takahashi et al., 2017*). 14-3-3 protein is known to bind to phosphoserine/threonine-containing proteins through amino acid binding motifs, including RxxpSxP (*Sluchanko et al., 2017*). 14-3-3 protein binds to the serine-30 residue of AKS1 only when Ser-30 is phosphorylated (*Takahashi et al., 2013*). The main components of the designed biosensor from N- to C- terminus end are the YPet (YFP variant) fluorescent protein (*Day and Davidson, 2009*), the 14-3-3 phosphopeptide-binding domain, 244 amino acids of an EV linker, 48 amino acids of the *Arabidopsis* AKS1 transcription factor and Turquoise GL cyan fluorescent protein (*Figure 1A*). As a control, we also generated a SNACS^{5785A} mutant isoform, in which the AKS1-Ser-30 residue is substituted with a non-phosphorylatable alanine (Ala) in the AKS1 domain.

A hypothetical simplified working model of the biosensor is outlined in *Figure 1B*: When the sensor is in an unphosphorylated state, the 14-3-3 domain was predicted to have a low affinity for the AKS1 substrate resulting in a low ratio of YPet to Turquoise GL fluorescent emission under the Turquoise GL excitation. However, when the AKS1 Ser-30 in this sensor is phosphorylated, the 14-3-3 domain was hypothesized to bind to the phosphorylated AKS1 region. Based on this working model, we tested this sensor to determine whether it can function as a readout of SnRK2 protein kinase activity.

We performed in vitro phosphorylation assays. The results showed that the OST1/SnRK2.6 protein kinase can phosphorylate this sensor, but not the SNACS-S785A mutant isoform (*Figure 1C*). Furthermore, the unrelated Ca²⁺-dependent protein kinase, CPK6, did not measurably phosphorylate the wild-type SNACS or S785A mutant (*Figure 1C*). To investigate whether this phosphorylation of SNACS might affect the FRET ratio (YPet emission/Turquoise GL emission), in vitro FRET assays were performed using recombinant SNACS and OST1/SnRK2.6 proteins. SNACS protein was incubated in the presence or absence of OST1/SnRK2.6 protein kinase, and then the fluorescence emission profile was determined in response to excitation at 434 nm. The SNACS showed an increase in YPet emission (average data points, 525–531 nm) by an average of 11.8% and a decrease of Turquoise GL emission (average data points, 471–477 nm) by 12.96% in the presence of OST1/SnRK2.6 compared to the SNACS alone upon Turquoise GL excitation (*Figure 1D*). This in vitro SNACS response appears to be nearly saturated under the imposed conditions, as incubation with two times the concentration of OST1/SnRK2.6 protein caused no further clear shift in the fluorescence



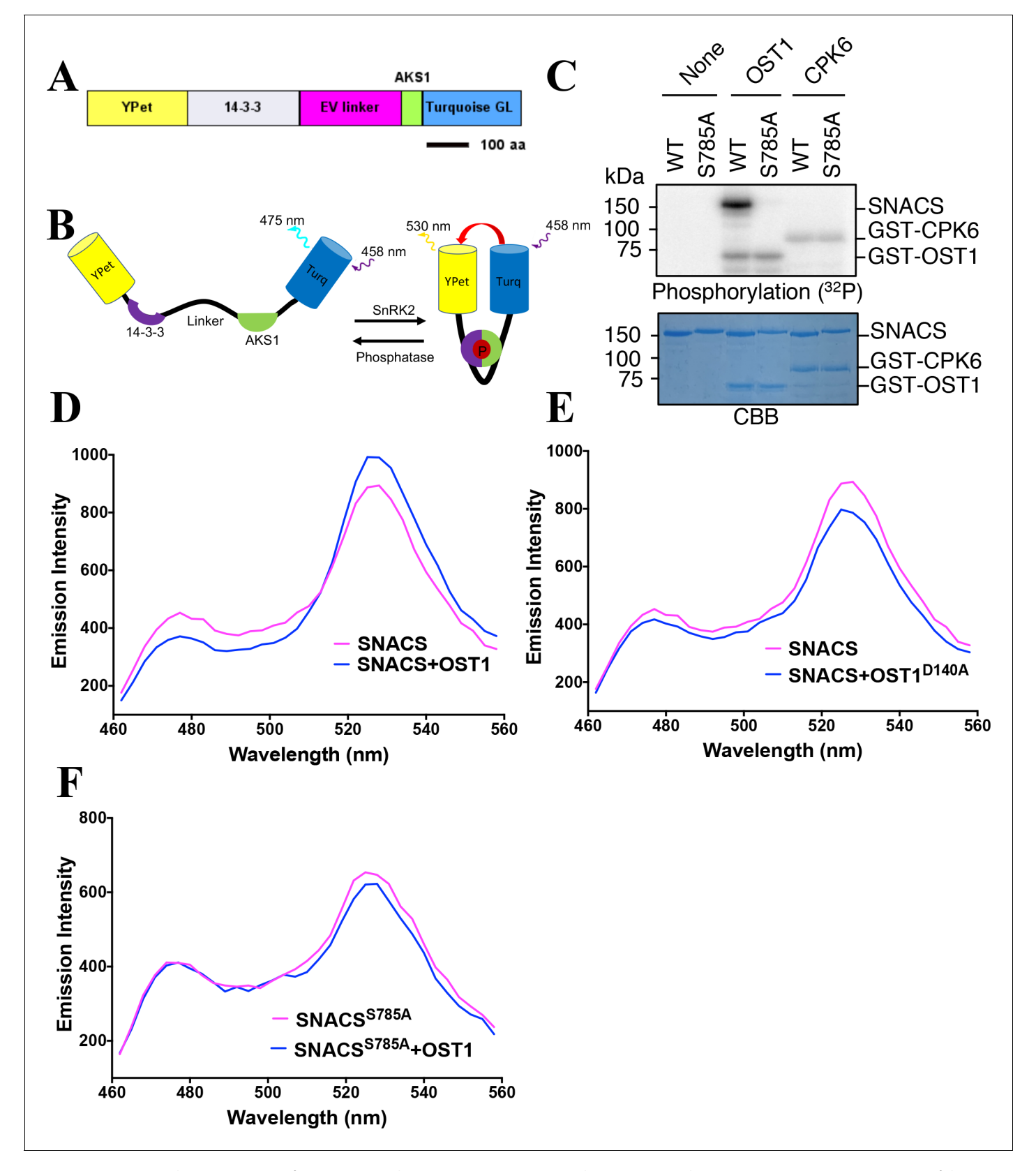


Figure 1. Structure and in vitro testing of SnRK2 protein kinase reporter, SNACS, and SnRK2 protein kinase activity. (A) Domain structure of the SNACS protein: YPet and Turquoise GL are yellow and cyan fluorescent proteins. The full coding region of the phosphoserine/threonine binding 14-3-3 GF14phi protein (At1g35160) was inserted, EV linker is a 244 amino acid length flexible linker domain, and AKS1 is a 48-amino-acid segment of the Figure 1 continued on next page



Figure 1 continued

Arabidopsis AKS1 transcription factor protein. aa, amino acid. (B) Simplified model of SNACS reporter function. Phosphorylation of the sensor within the AKS1 domain is predicted to produce a conformational shift that increases Förster resonance energy transfer (FRET) efficiency due to the enhanced affinity of the 14-3-3 domain for the phosphorylated form of the substrate domain. (C) In vitro phosphorylation assay. SNACS (WT) and SNACS^{5785A} (S785A) were incubated in the presence or absence of GST-OST1/SnRK2.6 protein kinase or GST-CPK6. Proteins were separated on a gel and the incorporation of ³²P into the substrates was evaluated via autoradiography (upper panel). The lower panel shows a loading control stained with Coomassie brilliant blue. (D) and (E) in vitro FRET assays using SNACS performed in the presence of GST-OST1 or GST-OST1 D140A (inactive OST1 kinase version). SNACS alone controls in D and E were from the same experiments shown in the two panels, as experiments were performed in parallel. The emission spectra of SNACS produced by excitation of the Turquoise GL domain with 434 nm light are shown. (F) In vitro FRET assays using SNACS^{5785A} mutant reporter performed in the presence or absence of GST-OST1. Emission spectra of the SNACS reporter produced by excitation of the Turquoise GL domain with 434 nm light are shown.

The online version of this article includes the following source data and figure supplement(s) for figure 1:

Source data 1. Uncropped gel images for Figure 1C.

Source data 2. In vitro SNACS FRET ratio values in Figure 1.

Figure supplement 1. In vitro FRET assay of SNACS reporter.

Figure supplement 1—source data 1. In vitro SNACS FRET ratio values in Figure 1—figure supplement 1.

spectrum (*Figure 1—figure supplement 1E*). In addition, in the presence of the inactive mutant isoform OST1/SnRK2.6 (OST1^{D140A}) protein kinase as a control, no clear FRET ratio increase was found (*Figure 1E* and *Figure 1—figure supplement 1A,B*). These results suggested phosphorylation of SNACS caused a FRET ratio increase.

Consistent with the above results, the mutant SNACS^{S785A} isoform with the AKS1 Ser-30-Ala mutation did not show FRET ratio changes after an incubation with the OST1/SnRK2.6 protein kinase upon Turquoise GL excitation (*Figure 1F* and *Figure 1—figure supplement 1C*). In additional experiments, SnRK2.3, another protein of SnRK2 family, induced a SNACS FRET ratio increase as well (*Figure 1—figure supplement 1D*). In contrast, the highly active CPK6 protein kinase (*Brandt et al., 2012*), did not increase the FRET ratio (*Figure 1—figure supplement 1D*). Taken together, these results indicate that SNACS shows an increase of FRET ratio based on a phosphorylation of the AKS1 domain by SnRK2 protein kinases in vitro. Furthermore, the AKS1 Ser-30-Ala mutation in SNACS disrupts this response in vitro (*Figure 1C,F* and *Figure 1—figure supplement 1C*).

SNACS reports SnRK2 activity dynamics in plant cells

We next investigated the functionality of SNACS in planta by performing live cell imaging. Transient expression experiments using the SNACS reporter in *Nicotiana benthamiana* were performed. SNACS driven by the cauliflower mosaic virus 35S promoter was co-expressed with *pUBQ10:OST1-6xHis-3xFLAG(HF)* (*Waadt et al., 2015*) in *Nicotiana benthamiana* by co-infiltration. Emission ratio images were recorded 3 days after infiltration. We immobilized abaxial intact leaf epidermal tissues on glass-bottom dishes, and then identified epidermal cells showing fluorescence. Interestingly, the application of ABA caused time-resolved emission ratio (YPet to Turquoise GL emission) increases in *N. benthamiana* epidermal cells (*Figure 2A,C,D*) (n = 3 experiments; 11–13 cells imaged in each experiment). As ABA was dissolved in 0.02% EtOH, EtOH was used as a solvent control. EtOH treatments did not induce measurable emission ratio increases of SNACS (*Figure 2B*, n = 3 experiments; 4–7 cells imaged in each experiment).

SNACS and the mutant control isoform SNACS^{S785A} were also stably transformed into *Arabidopsis*. Two independent transgenic lines were characterized for each of the two sensor constructs. SNACS fluorescence was observed throughout plant seedlings in the *35S:SNACS* expression lines, including guard cells and leaf epidermal cells (*Figure 2—figure supplement 1*). We tested effects of ABA on these sensors in stomatal guard cells. To conduct non-biased experiments, ABA or EtOH treatments were blinded in these assays and in these data analyses. Using a genetic background in which a tagged version of OST1 was expressed in the *OST1* T-DNA insertion allele *ost1-3* (*pUBQ10*: *OST1-HF/ost1-3*) (*Yoshida et al., 2002*; *Waadt et al., 2015*), application of 20 µM ABA induced a clear time-dependent increase in the FRET ratio, which reached stable saturation 2 to 4 min after application (*Figure 3A,C* to E, p=0.015, paired t-test, before ABA time point 3 min vs. after ABA time point 10 min; All following imaging analyses were evaluated by paired t-tests). Ethanol control



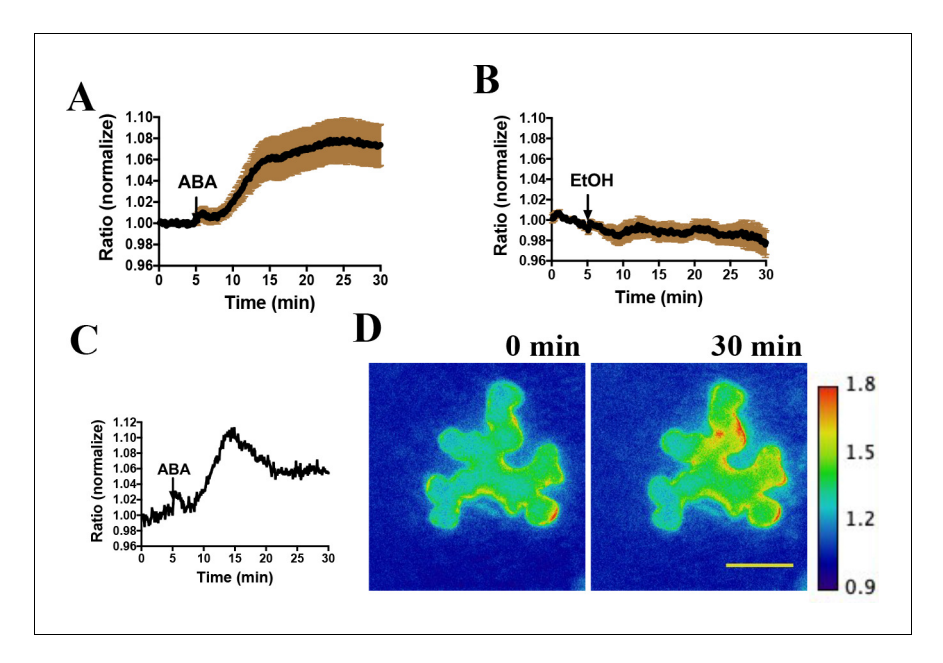


Figure 2. Abscisic acid induces increases in the ratio of YPet to Turquoise GL fluorescence emission of the SNACS reporter in *N. benthamiana*. (A) Time-resolved FRET ratio changes in response to ABA. SNACS was co-infiltrated with $\rho UBQ10:OST1-HF$ in *N. benthamiana*. Leaf epidermises were perfused with assay buffer (5 mM KCl, 50 μM CaCl₂, 10 mM MES-Tris, pH 5.6) and then 20 μM ABA was added as indicated by the arrow. Experiments were repeated at least three times with similar results. FRET efficiency changes were recorded by measuring the ratio of fluorescence emissions at 535 nm/480 nm with an excitation wavelength of 434 nm (see Materials and methods). Data are averages of normalized emission ratios of YPet to Turquoise GL emission produced by exciting Turquoise GL from 11 cells. Error bars denote mean ± SEM. (B) Time-resolved FRET ratio in response to 0.02% EtOH (solvent control for ABA). Data are averages of normalized emission ratios from 7 cells. Error bars denote mean ± SEM. (C) and (D) Example of a single cell experiment from A. (C) The corresponding emission ratio normalized to the average value over 5 min before treatment. (D) Pseudo-colored fluorescence ratio images of SNACS-expressing *N. benthamiana* leaf epidermal cells at times 0 min and 30 min. The calibration bar to the right of (D) indicates the numerical ratio (non-normalized) scale corresponding to the heat map. Bar = 50 μm.

Source data 1. SNACS FRET ratio values from each stomate in Figure 2.

Figure supplement 1. Ratiometric image of 535/480 nm wavelength emissions show fluorescence in SNACS-expressing *Arabidopsis* epidermal cells (pseudo-colored fluorescence ratio scale is shown on the right, non-normalized).

applications showed no clear YPet/Turquoise GL emission ratio change (*Figure 3B*). Image analyses suggest that SNACS protein is either absent from the nucleus or is expressed at lower levels than in the cytoplasm, with fluorescence possibly 'bleeding through' from the cytoplasm to the nucleus (*Figure 3—figure supplement 1*).

Similar to the above experiments (*Figure 3*), in the Col-0 (wild-type) background, expression of SNACS showed ABA-induced emission ratio increases in guard cells (*Figure 4A and D*, n = 24 stomata, $p=2 \times 10^{-12}$ 3 min vs. 10 min time points). In additional experiments sets, expression of SNACS in the *pUBQ10:OST1-HF/ost1-3* background also showed ABA-induced emission ratio change (*Figure 4E and H*, n = 16 stomata, $p=1.4 \times 10^{-7}$ 3 min vs. 10 min). In transgenic lines expressing the mutant SNACS^{S785A}, that corresponds to the Ser-30-Ala mutation in AKS1, no clear increases in the ratio of YPet to Turquoise GL emission ratio were observed after ABA application (*Figure 4C and G*; n = 9 stomata (4C), p=0.892, 3 min vs. 10 min; n = 12 stomata (4G), p=0.184, 3 min vs. 10 min). These data indicate that the phosphorylation site Ser 785 residue of SNACS (*Figure 4C and G*) is necessary for ABA-induced increases in the ratio of YPet to Turquoise GL emission in plant cells. In additional EtOH application controls, both in SNACS and in SNACS^{S785A} expressing transgenic lines no substantial EtOH-induced increases were observed in the ratio of YPet to Turquoise GL emission (*Figure 4B,F* and *Figure 4—figure supplement 1*; n = 9 stomata



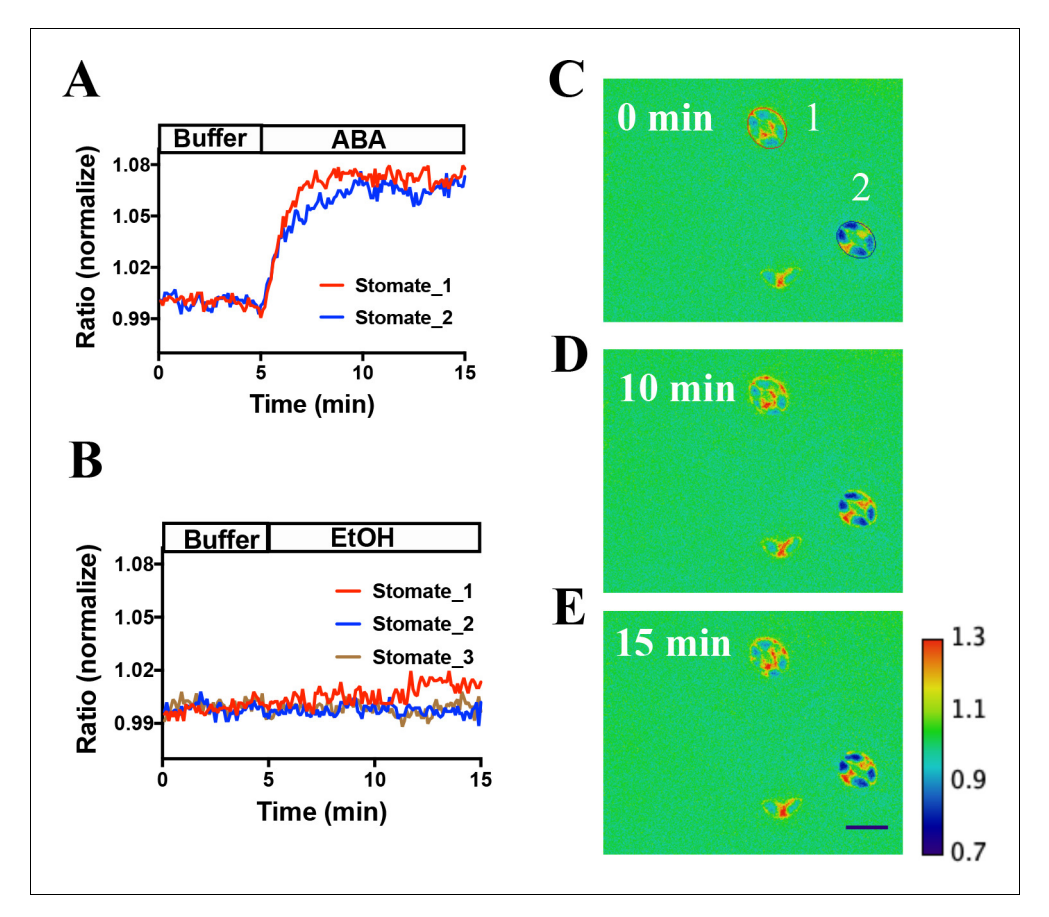


Figure 3. In vivo response of SNACS reporter of SnRK2 activity in response to ABA in *Arabidopsis* guard cells. (A) Time-resolved FRET ratio changes in response to ABA (20 μM). FRET efficiency changes were recorded by measuring the ratio of fluorescence emissions at 535 nm/480 nm with an excitation wavelength of 434 nm (see Materials and methods). (B) Time-resolved FRET ratio change in response to EtOH (0.02%, solvent control for ABA). (C to E) Images of SNACS fluorescence ratios in guard cells from A at 0 min, 10 min and 15 min. The colored circles indicate the regions of interest (ROIs) used to measure fluorescence emissions with the colors corresponding to the blue and red traces in panel A. '1' and '2' in (C) denote 'stomate_1' and 'stomate_2', respectively. The calibration bar in the lower right of (E) indicates the numerical scale corresponding to the nonnormalized heat map. Bar = $20 \, \mu m$. Note that the lowest cell (red spot) in the images shows fluorescence of a single guard cell from an apparent half stomate. Treatments were performed blinded (ABA or EtOH). SNACS FRET activities in guard cells in leaf epidermises were analyzed in a *pUBQ10:OST1-HF*-expressing *ost1-3* genetic background (*Waadt et al., 2015*). The ratio of YPet to Turquoise GL emission was normalized to the average value over 5 min before treatment.

The online version of this article includes the following source data and figure supplement(s) for figure 3:

Source data 1. SNACS FRET ratio values from each stomate in Figure 3.

Figure supplement 1. SNACS fluorescence appears to be observed mainly in the cytoplasm, with possible low expression in the nucleus or fluorescence may 'bleed' from the cytoplasm towards the nuclear region.

(4B), p=0.808, 3 min vs. 10 min; n = 11 stomata (4F), p=0.112, 3 min vs. 10 min). Average time-dependent ratiometric fluorescence changes for data including data in **Figure 4** are shown in **Figure 4**—**figure supplement 2A–H**.

We next investigated whether the SNACS ratio change was dependent on SnRK2 activity in planta. As SnRK2.2, SnRK2.3 and SnRK2.6 have been shown to contribute to ABA signaling in guard cells (*Takahashi et al., 2017*; *Fujii and Zhu, 2009*; *Brandt et al., 2015*; *Takahashi and Kinoshita, 2015*), we examined SNACS in Col-0, ost1/snrk2.6 single mutant, snrk2.2/2.3 double mutant and snrk2.2/2.3/2.6 triple mutant plants (*Figure 5*). Interestingly, ABA caused clear fluorescence emission ratio increases in ost1/snrk2.6 guard cells (*Figure 5B*; n = 14 stomata, p=3.2 \times 10⁻⁷ 3 min vs. 10 min). Compared to the Col-0 guard cells, in the ost1/snrk2.6 background ABA induced slower



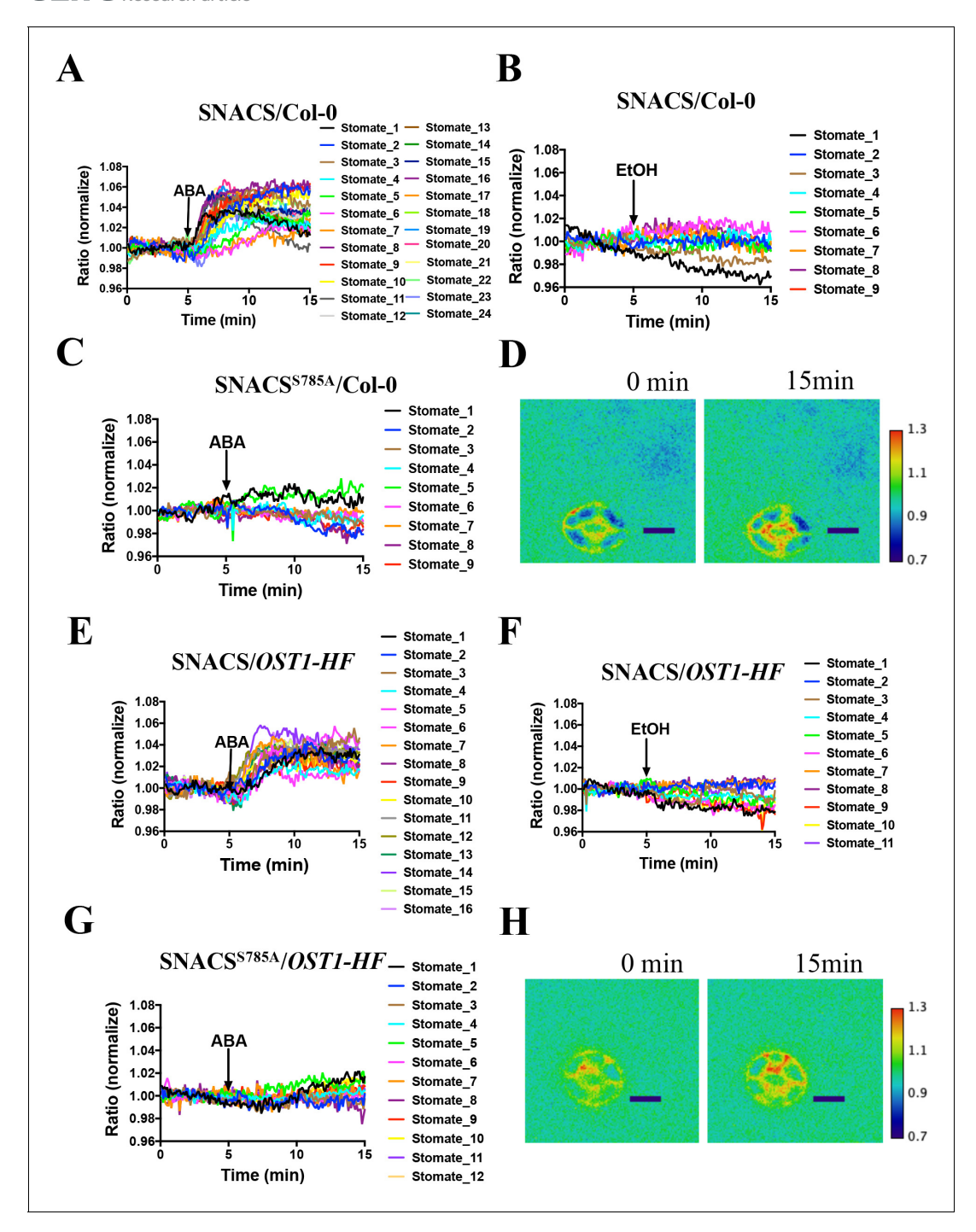


Figure 4. The amino acid AKS1 Ser-30 in the SNACS reporter is necessary for ABA-induced ratio increases in *Arabidopsis* guard cells. Leaf epidermises from transgenic lines expressing SNACS were used for depicting the ratio of YPet to Turquoise GL emission produced by exciting Turquoise GL with 434 nm light. (A) ABA (20 μM) induced the SNACS response in the Col-0 genetic background. (B) SNACS response to EtOH (0.02%, solvent control for ABA) treatment in the Col-0 wild-type genetic background. (C) The S785A mutation in the SNACS reporter impairs ABA-induced FRET ratio changes in the Col-0 wild-type genetic background. (D) A representative SNACS fluorescence ratio image from A at 0 min and 15 min time points. Bar = 10 μm. (E) ABA (20 μM) induced SNACS response in the *pUBQ10:OST1-HF*-expressing in *ost1-3* genetic background. (G) The S785A mutation in the SNACS impairs ABA-induced FRET ratio changes in the *pUBQ10:OST1-HF*-expressing in *ost1-3* genetic background. The ratios were normalized to the average value over the 5 min before treatment. (H) A representative SNACS fluorescence ratio image from E at 0 min and 15 min time points. Bar = 10 μm. Calibration bars to the right of D and H show the numerical ratio (non-normalized) scale corresponding to the pseudo-coloring. The online version of this article includes the following source data and figure supplement(s) for figure 4:

Figure 4 continued on next page



Figure 4 continued

Source data 1. SNACS FRET ratio values from each stomate in Figure 4.

Figure supplement 1. EtOH controls for SNACS^{S785A} in Col-0 and in pUBQ10:OST1-HF expressed in the ost1-3 genetic background.

Figure supplement 1—source data 1. SNACS FRET ratio values from each stomate in Figure 4—figure supplement 1.

Figure supplement 2. Combined and averages of single stomate imaging data from experimental sets including experiments in Figure 4.

Figure supplement 2—source data 1. SNACS FRET ratio values from each stomate in Figure 4—figure supplement 2.

emission ratio increases (*Figure 5A and B*; n = 12 stomata (5A), p= 2.4×10^{-6} 3 min vs. 10 min). In *snrk2.2/2.3* double mutant guard cells, ABA induced FRET ratio increases were observed (*Figure 5C*, n = 20 stomata (5C), p= 5.7×10^{-9} 3 min vs. 10 min). Notably, no ABA-induced ratio increase was observed in the *snrk2.2/2.3/2.6* triple mutant guard cells, which suggests that SnRK2

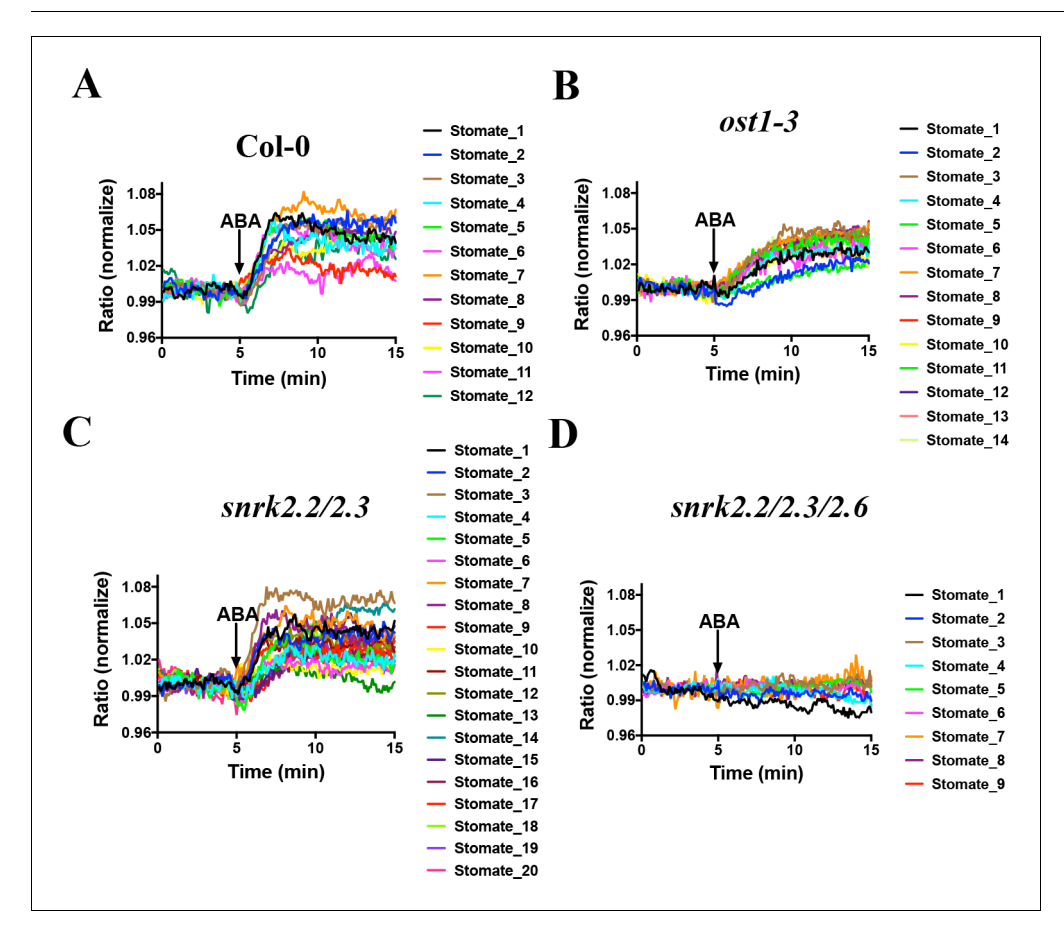


Figure 5. SnRK2 activity is needed in guard cells for ABA-induced increases in the FRET ratio of SNACS. Leaf epidermises from transgenic lines expressing SNACS were used for analyzing the ratio of YPet to Turquoise GL emission in guard cells produced by exciting Turquoise GL with 434 nm light. The ratio was normalized to the average value over the 5 min before ABA exposure. (A) ABA (20 μM) induced SNACS responses in guard cells of the Col-0 (WT) genetic background. (B) ABA (20 μM) induced SNACS responses in guard cells of the ost1-3 genetic background. (C) ABA (20 μM) induced SNACS responses in guard cells of the snrk2.2/2.3 double mutant genetic background. (D) ABA (20 μM) induced SNACS response was impaired in snrk2.2/2.3/2.6 triple mutant guard cells.

The online version of this article includes the following source data and figure supplement(s) for figure 5:

Source data 1. SNACS FRET ratio values from each stomate in Figure 5.

Figure supplement 1. Combined and averages of single stomate imaging data from experimental sets shown in *Figure 5*.

Figure supplement 1—source data 1. SNACS FRET ratio values from each stomate in Figure 5—figure supplement 1.



activity is required for ABA-induced SNACS-dependent FRET ratio changes in planta (*Figure 5D*, n = 9 stomata, p=0.122 3 min vs. 10 min). Average time-resolved fluorescence emission data from *Figure 5* are shown in *Figure 5*—*figure supplement 1*. These data are consistent with findings that all three SnRK2s contribute to ABA signaling in guard cells and that the triple mutant has the strongest physiological phenotype (*Fujii and Zhu, 2009*; *Brandt et al., 2015*). Taken together, these data provide strong evidence that time-dependent SnRK2 activity can be detected in single live cells by SNACS both in *N. benthamiana* and *Arabidopsis*.

Effects of kinase inhibitors on SNACS

Previous research has led to the hypothesis that basal ABA signaling and basal SnRK2 activity occur in non-stressed guard cells (Hsu et al., 2018; Yoshida et al., 2019; Lahr and Raschke, 1988). However, experimental evidence directly examining the proposed basal activity of SnRK2 kinases in intact guard cells is lacking. Experiments were pursued to determine the effects of protein kinase inhibition during SNACS recordings. In order to determine the effects of kinase inhibition, the general Ser/Thr protein kinase inhibitor, K252a was used, which abolishes ABA-induced stomatal closing (Schmidt et al., 1995). We found that 10 µM K252a application resulted in a time-resolved drop in the FRET emission ratio in Arabidopsis guard cells (Figure 6A; n = 13 stomata (6A), p=4.9 \times 10⁻⁶ 3 min vs.10 min; n = 11 stomata (6B, controls), p=0.158 3 min vs. 10 min). In addition, ABA did not induce measurable emission ratio increases after K252a application, suggesting that ABA-induced emission ratio increases are caused by K252a-sensitive protein kinase activity in vivo (Figure 6A). Next, we added 10 µM K252a following 10 min ABA treatments. Interestingly, after ABA treatment and subsequent K252a exposure, the FRET emission ratio decreased, suggesting that SNACS can reversibly report protein kinase activity (Figure 6C; n = 10 stomata (6C), p=0.0004 3 min vs.10 min, p=0.0001 10 min vs. 20 min; n = 8 stomata (6D, controls), p=0.00003 3 min vs.10 min, p=0.836 10 min vs. 20 min).

As control, we tested whether the calmodulin inhibitor W7 affects SnRK2 protein kinase activity in plant cells. *In-gel* kinase assays showed that W7 does not have a clear effect on ABA-induced OST1/SnRK2.6 activation in *Arabidopsis* mesophyll cell protoplasts (*Figure 6—figure supplement 1*). In controls K252a inhibited ABA-induced *in-gel* kinase activity (*Figure 6—figure supplement 1*). For comparison to the K252a inhibitor, we investigated the effect of W7 (*Rudd et al., 1996*) on the SNACS reporter in guard cells. We found no FRET ratio changes upon W7 treatment (*Figure 6E and F*; n = 8 stomata (6E), p = 0.988 3 min vs.10 min; n = 7 stomata (6F, controls), p = 0.348 3 min vs.10 min). After W7 exposure, application of ABA caused ABA-induced FRET shifts (*Figure 6E and F*; $p = 1.1 \times 10^{-9}$ (6E), $p = 7.4 \times 10^{-6}$ (6F), 10 min vs. 20 min). Average time-resolved fluorescence emission ratio changes are shown in *Figure 6—figure supplement 2* that include the data in *Figure 6*. Taken together, these data suggest that SNACS is a reversible protein kinase activity reporter and that SNACS can report basal SnRK2 activity in vivo, that is down-regulated upon kinase inhibition.

Methyl-Jasmonate does not induce SNACS FRET ratio changes in guard cells

Methyl jasmonate (MeJA) has been previously reported to induce stomatal closure (*Herde and Pena-Cortes, 1997*; *Gehring, 1997*; *Suhita et al., 2004*; *Akter et al., 2012*). The OST1/SnRK2.6 kinase is required for MeJA-induced stomatal closure (*Yin et al., 2016*). Therefore, next we analyzed the effect of MeJA on SNACS FRET changes in guard cells. Exogenous application of MeJA did not result in robust FRET emission ratio changes in *Arabidopsis* guard cells (*Figure 7, Figure 7—figure supplement 1*; n = 9 stomata (7A), p=0.981 3 min vs. 15 min, p=0.896 3 min vs. 25 min; n = 12 stomata (7B, controls), p=0.553 3 min vs. 15 min, p=0.664, 3 min vs. 25 min). Furthermore, in the presence of MeJA, subsequent application of ABA caused increases in the SNACS emission ratio in these experiments (*Figure 7*).

CO₂ elevation does not induce SNACS FRET ratio increases in guard cells

snrk2.6/ost1 mutant alleles show impaired and slowed CO_2 -induced stomatal closure (**Xue et al., 2011**; **Merilo et al., 2013**; **Hsu et al., 2018**). Interestingly, a recent study suggests that CO_2 elevation does not activate SnRK2.6/OST1 protein kinases using *in-gel* kinase assays with isolated



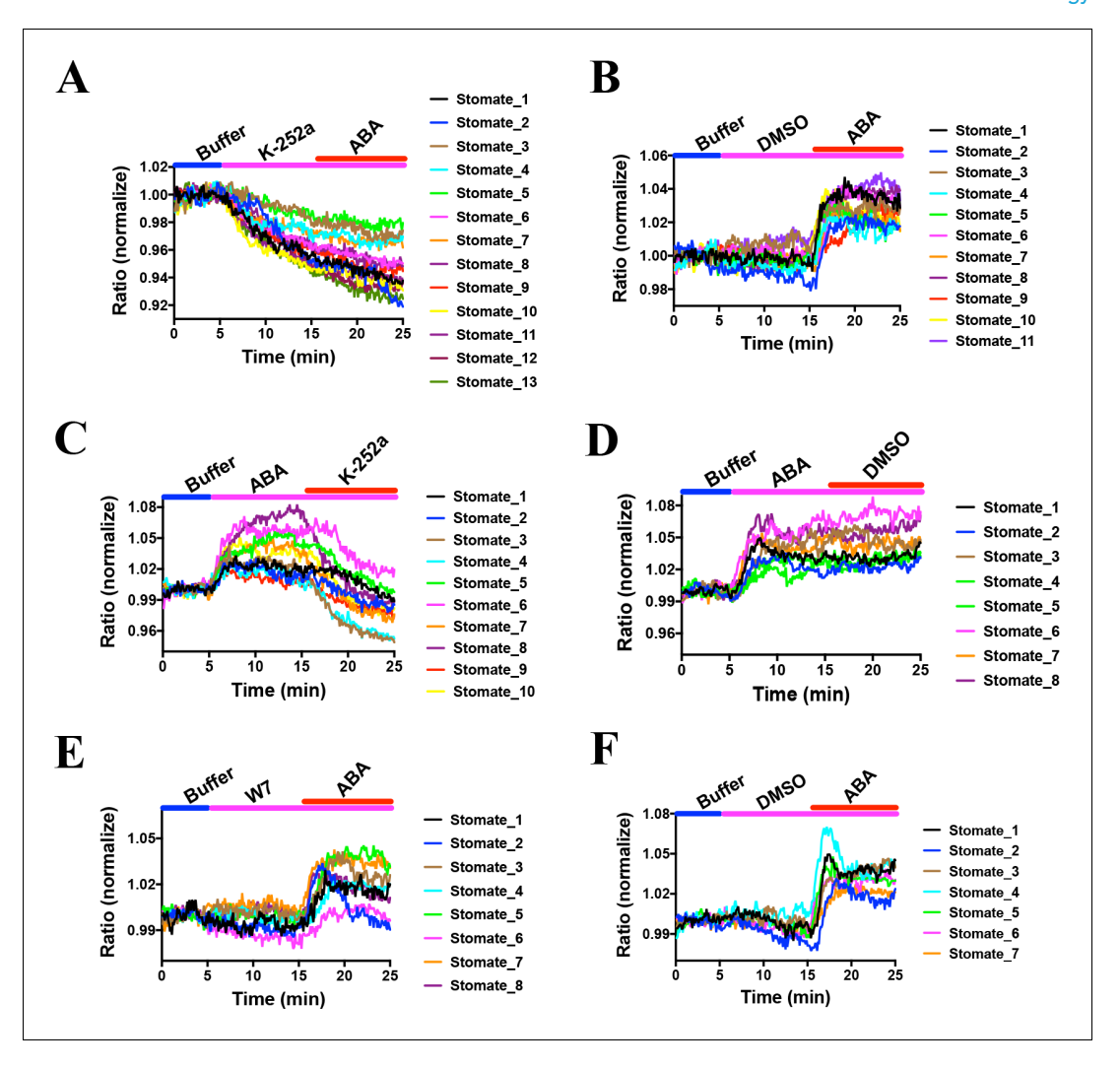


Figure 6. Effects of kinase inhibitors on SNACS fluorescence emission ratios in guard cells. SNACS responses in guard cells were analyzed in the pUBQ10:OST1-HF-expressed in the ost1-3 genetic background. The ratio of YPet to Turquoise GL emission was normalized to the average value over the 5 min before K252a application. (A) The protein kinase inhibitor K-252a reduced SNACS FRET ratio in vivo, and ABA did not induce a ratio increase in the presence of K-252a. After 10 min incubation with 10 μM K-252a, 20 μM ABA was added. (B) ABA induced a ratio increase in the presence of DMSO (0.2%, solvent control for K-252a). (C) The kinase inhibitor K-252a inhibited SnRK2 kinase activity after ABA treatment. (D) Control experiment for C. 0.2% DMSO was added. (E) Kinase inhibitor W7 did not affect SNACS FRET ratio in vivo. After 10 min incubation with 20 μM W7, 20 μM ABA was added. (F) Control experiment for E. 0.1% DMSO was added as solvent for W7.

The online version of this article includes the following source data and figure supplement(s) for figure 6:

Source data 1. SNACS FRET ratio values from each stomate in Figure 6.

Figure supplement 1. W-7 does not have a clear effect on ABA-induced OST1/SnRK2.6 activation in plant cells.

Figure supplement 1—source data 1. Uncropped gel images for Figure 6—figure supplement 1.

Figure supplement 2. Combined and averages of single stomate imaging data from experimental sets including experiments in *Figure 6*.

Figure supplement 2—source data 1. SNACS FRET ratio values from each stomate in Figure 6—figure supplement 2.

Arabidopsis guard cell protoplasts (Hsu et al., 2018). However, based on the present debate whether CO₂ elevation directly activates early ABA signal transduction (Dittrich et al., 2019) or not (Hsu et al., 2018; Merilo et al., 2013), real-time analyses in intact guard cells are needed. Here, using SNACS-expressing Arabidopsis plants, we tested whether changes in CO₂ concentration affect SNACS FRET activity in intact guard cells in real-time analyses. Intact leaf epidermises (Young et al.,



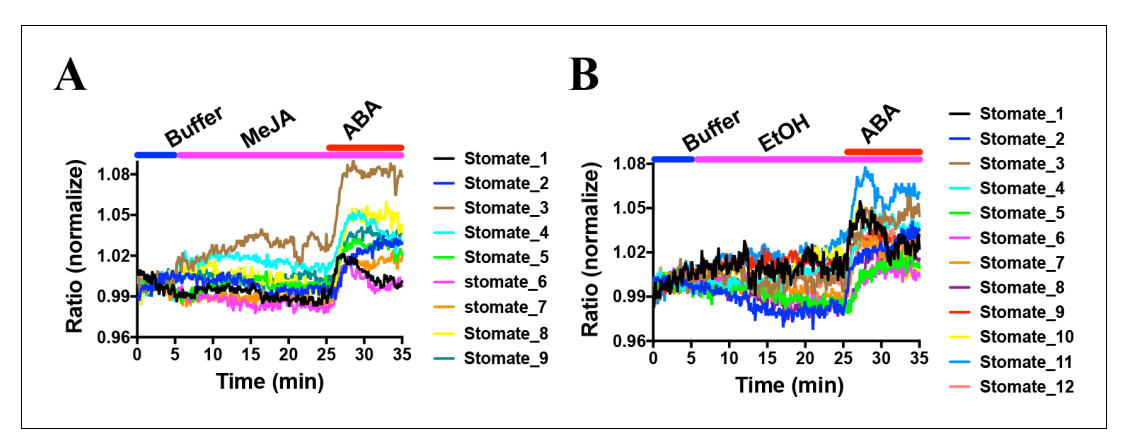


Figure 7. MeJA did not induce consistent FRET ratio changes of the SNACS SnRK2 activity reporter in guard cells under the imposed conditions. The SNACS reporter was analyzed in guard cells in leaf epidermises of plants expressing pUBQ10:OST1-HF in the ost1-3 genetic background. The ratio of YPet to Turquoise GL emission was normalized to the average value over the 5 min before treatment. (A) MeJA (20 μM) did not affect the FRET ratio in guard cells. ABA induced ratio increases in the presence of MeJA. After 20 min treatment with 20 μM MeJA, 20 μM ABA was added. (B) Control experiment for A. 0.1% EtOH (solvent control for MeJA) was added. The online version of this article includes the following source data and figure supplement(s) for figure 7:

Source data 1. SNACS FRET ratio values from each stomate in *Figure 7*.

Figure supplement 1. Combined and averages of single stomate imaging data from experimental sets including experiments in *Figure 7*.

Figure supplement 1—source data 1. SNACS FRET ratio values from each stomate in Figure 7—figure supplement 1.

2006) were incubated in a low CO_2 buffer (115 ppm) for 10 min, and the buffer was replaced with a high CO_2 buffer (1170 ppm) by perfusion while monitoring SNACS FRET ratios. FRET emission ratios showed no measurable increases after a 40 min incubation with the high CO_2 buffer (*Figure 8A* and *Figure 8—figure supplement 1A*, n=9 stomata, p=0.184 3 min vs. 15 min). After high CO_2 treatment, 20 μ M ABA was added to the buffer. We observed rapid FRET ratio increases in response to ABA (*Figure 8A*). Low CO_2 causes a rapid opening of stomatal pores. We further tested whether low CO_2 disrupts ABA-induced FRET ratio changes of the SNACS reporter. No clear FRET ratio increases were detected for continuous 30 min low CO_2 exposure (115 ppm). Subsequent exposure to 20 μ M ABA caused ratio increases (*Figure 8B* and *Figure 8—figure supplement 1B*, n=14 stomata, $p=5.9 \times 10^{-6}$ 20 min vs. 35 min).

CO₂-induced stomatal closing is >80% completed within 15 to 20 min of a CO₂ concentration elevation in wild-type (Col-0) Arabidopsis (Young et al., 2006). In previous research using the ABA nano-reporter ABAleon2.15, a shift in the CO2 concentration from 115 ppm to 535 ppm did not cause a measurable increase in the ABA concentration in guard cells, even though ABA receptors and OST1 were found to be important for the CO2 response (Hsu et al., 2018), which was differently interpreted in a recent study (Dittrich et al., 2019). Nevertheless, we pursued experiments here to determine whether a shift to a higher CO₂ concentration of 1170 ppm could cause a rapid increase in the ABA concentration in guard cells. No dramatic ABAleon2.15 emission ratio change was observed upon increasing the CO₂ concentration from 115 ppm to 1170 ppm (Figure 8C and Figure 8-figure supplement 1C, n = 10 stomata, p=0.502 3 min vs. 30 min). At the end of these experiments, intact abaxial leaf epidermises were exposed to 20 µM ABA, which caused a rapid reduction in the ABAleon2.15 FRET ratio (Figure 8C,D and Figure 8—figure supplement 1C), which corresponds to an increase in cellular ABA concentration (Waadt et al., 2014). In control experiments, no detectable emission ratio change was observed in 30 min of low CO₂ buffer exposure (115 ppm), followed by a rapid reduction in ratio upon exposure to 20 µM ABA (Figure 8D and Figure 8—figure supplement 1D; n = 9 stomata, p=6.1 \times 10⁻⁷20 min vs. 35 min). Thus, no clear rapid increase in the cellular ABA concentration of guard cells was found within the time frame in which CO₂-induced stomatal closing occurs.



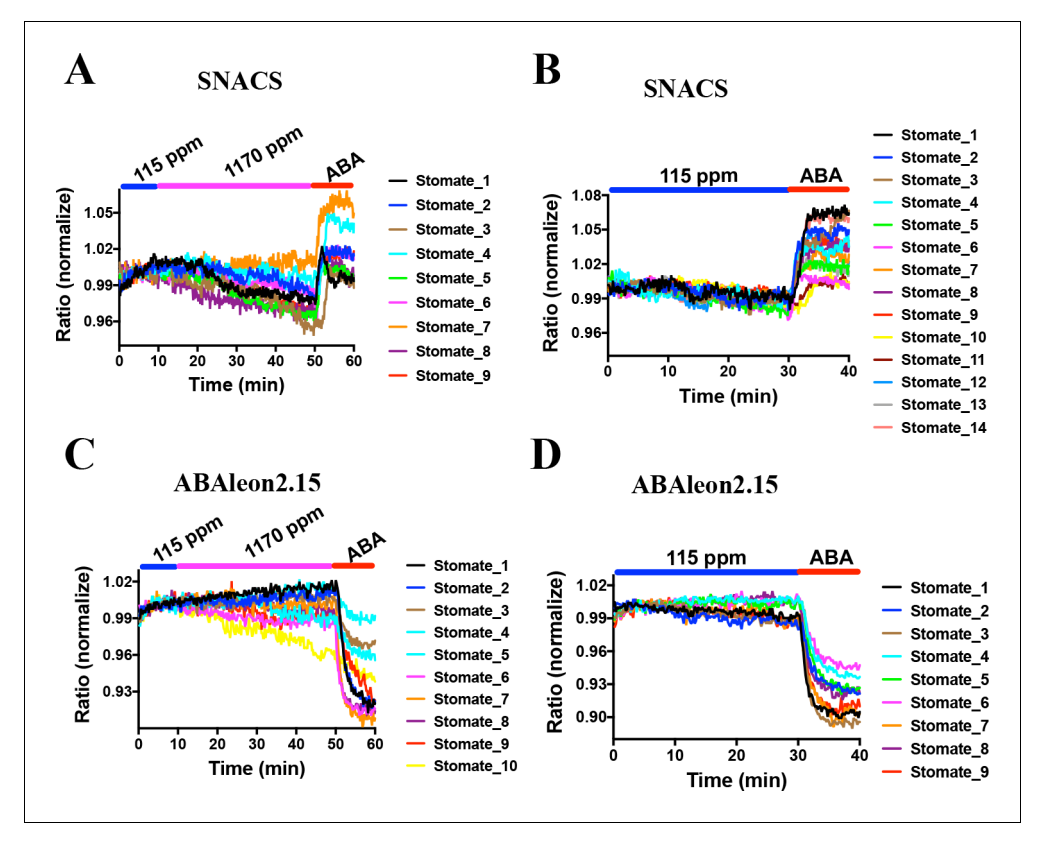


Figure 8. CO $_2$ elevation neither induces SNACS FRET ratio increases nor affects ABA concentration in guard cells. Fluorescence ratios of guard cells in intact leaf epidermises were analyzed in the *pUBQ10:OST1-HF* expressed in the *ost1-3* genetic background (**A and B**). The ratio of YPet to Turquoise GL emission was normalized to the average value over the 10 min before treatments. (**A**) High CO $_2$ (1170 ppm) did not increase the FRET ratio in guard cells. Intact leaf epidermises were exposed to low CO $_2$ (115 ppm), then switched to high CO $_2$ (1170 ppm) buffer, and then exposed to 20 μ M ABA containing buffer. (**B**) Leaf epidermises were exposed to low CO $_2$ (115 ppm), then exposed to 20 μ M ABA containing buffer. (**C**) Time-resolved ABAleon2.15 emission ratios in guard cells in response to CO $_2$ changes and ABA application. Intact leaf epidermises were exposed to low CO $_2$ (115 ppm), then switched to high CO $_2$ (1170 ppm) buffer, and then exposed to 20 μ M ABA containing buffer. (**D**) Leaf epidermises were exposed to low CO $_2$ (115 ppm), then exposed to 20 μ M ABA containing buffer. Note that reduction in fluorescence ratios observed in ABAleon2.15-expressing guard cells correspond to ABA concentration increases (*Waadt et al., 2014*).

The online version of this article includes the following source data and figure supplement(s) for figure 8:

Source data 1. SNACS FRET ratio values from each stomate in Figure 8.

Figure supplement 1. Combined and averages of single stomate imaging data from experimental sets including experiments in *Figure 8*.

Figure supplement 1—source data 1. SNACS FRET ratio values from each stomate shown in Figure 8—figure supplement 1.

PYL4 and PYL5 ABA receptors are not essential for CO₂-induced stomatal closing

A recent study has suggested that CO₂-induced stomatal closing requires PYL4 and PYL5 ABA receptors (*Dittrich et al., 2019*). As the present study has found no clear CO₂ activation of SnRK2s in guard cells and no CO₂-induced ABA increases in guard cells, we pursued gas exchange experiments in intact plants with mutants lacking *PYL4* and *PYL5* expression. Experiments were conducted on higher order ABA receptor mutants that have been shown to disrupt ABA-induced stomatal closing (*Merilo et al., 2018*; *Gonzalez-Guzman et al., 2012*). Experiments were performed in quintuple ABA receptor mutants: *pyr1 pyl1 pyl4 pyl5 pyl8* ('*pyl-11458*') and *pyr1 pyl2 pyl4 pyl5 pyl8* ('*pyl-12458*').



Time-resolved gas exchange experiments measuring whole intact plants showed that all tested plant lines displayed stomatal closure in response to changing the CO₂ concentration from ambient (400 ppm) to 800 ppm (Figure 9A and B). Earlier studies have shown the crucial role of PYR/RCAR receptors in maintaining steady-state stomatal conductance (Hsu et al., 2018; Gonzalez-Guzman et al., 2012; Merilo et al., 2013). ABA receptor sextuple mutant plants displayed 5.2 times higher pre-CO2-treatment stomatal conductance compared to wild-type (Figure 9A and C). ABA receptor quintuple pyl-11458 and pyl-12458 mutants maintained 2.3 and 2.9 times higher pretreatment stomatal conductances compared to wild-type (Figure 9A and C). After application of elevated CO2, the stomatal conductance of all ABA receptor mutant lines decreased to a similar or even higher extent than in wild-type plants even though their stomatal conductances remained higher after 50 min in elevated CO₂ (Figure 9A and C). This can be in part explained by an increased stomatal density in higher order ABA receptor knockout mutants and a weaker response to basal ABA concentrations (Hsu et al., 2018; Merilo et al., 2018). Stomatal responses to CO2 shifts from 400 to 800 ppm were clearly delayed in PYR/RCAR sextuple mutant plants as indicated by a roughly twice longer half-response time (Figure 9D), consistent with previous findings (Hsu et al., 2018). We also calculated reductions in stomatal conductance after 20 min under elevated CO₂ as an approximation for the initial phase of the CO₂ responses (Figure 9—figure supplement 1). Such analyses showed that in absolute units PYR/RCAR quintuple mutant pyl-12458 and sextuple mutant pyl-112458 plants displayed a larger absolute reduction in stomatal conductance in response to high CO₂ than wild-type plants.

To further investigate the role of PYL4 and PYL5 in CO₂-induced stomatal closing, we pursued a light protocol followed by CO₂ elevation, as in experiments used by *Dittrich et al., 2019*. In these experiments, *pyl-11458* quintuple mutant leaves showed stomatal opening in response to 125 μmol m⁻² s⁻¹ light as expected. After light-induced stomatal opening, CO₂ elevation showed similar CO₂-induced stomatal closing in the wild-type (Col-0) background as in the *pyl-11458* quintuple mutant that lacks *PYL4* and *PYL5* (*Figure 9—figure supplement 2A*). In complementation lines expressing *PYL4*, *PYL5* or *PYL1* under control of the guard cell *pGC1* promoter, no clear enhancement of the final CO₂ response was observed (*Figure 9—figure supplement 2B* to D). Thus in the two laboratories in which CO₂-regulation of stomatal conductance was investigated in intact plants in the present study (EM and HK lab and JS lab), we could not confirm that the absence of PYL4 and PYL5 disrupts the stomatal CO₂ response (*Dittrich et al., 2019*).

Discussion

In plants, SnRK2 protein kinases play critical roles in abiotic stress responses (Boudsocq and Laurière, 2005; Umezawa et al., 2009; Nakashima et al., 2009; Fujita et al., 2009; Fujii and Zhu, 2009; Li et al., 2000; Yoshida et al., 2002; Mustilli et al., 2002). Abscisic acid activation of SnRK2 protein kinases is required for ABA signal transduction (Cutler et al., 2010; Raghavendra et al., 2010; Zhu, 2016). However, the common, in-gel SnRK2 kinase assay method has significant limitations for monitoring cell type, cellular compartment and time-dependent activation of these protein kinases. In-gel kinase assays in Arabidopsis guard cells require purification of 10⁵ or more guard cell protoplasts from more than 100 leaves and 10 plants for each individual guard cell in-gel kinase assay lane. Real-time FRET measurements of SnRK2 protein kinase activities in intact individual plant cells and tissues using the SNACS reporter enable direct investigation of key biological questions in real time, as shown here.

In this study, we developed a SnRK2 protein kinase sensor, SNACS, containing an AKS1 substrate domain and a full length 14-3-3 protein. The SnRK2.6/OST1 kinase phosphorylated the SnRK2 sensor in dependence of the AKS1 Ser-30 residue in vitro (*Figure 1C*), which is essential for 14-3-3 protein binding in ABA signal transduction (*Takahashi et al., 2013*). In vitro and in planta analyses show an increase in FRET ratio in a SnRK2 kinase activity-dependent manner (*Figures 1D,E* and *5*). We further observed ABA-induced FRET ratio increases in *Nicotiana benthamiana* epidermal cells and *Arabidopsis* guard cells (*Figures 2* and *3*). Phosphorylation of the AKS1 Ser-30 residue is required for 14-3-3 protein binding to the AKS1 protein (*Takahashi et al., 2013*). Notably, the mutant AKS1 Ser-30-Ala sensor isoform does not show FRET ratio changes both in vitro and in plant cells (*Figures 1F* and *4*). These results are consistent with a model in which changes in FRET ratio are derived from a conformational change through 14-3-3 protein binding to the phosphorylated AKS1 domain in



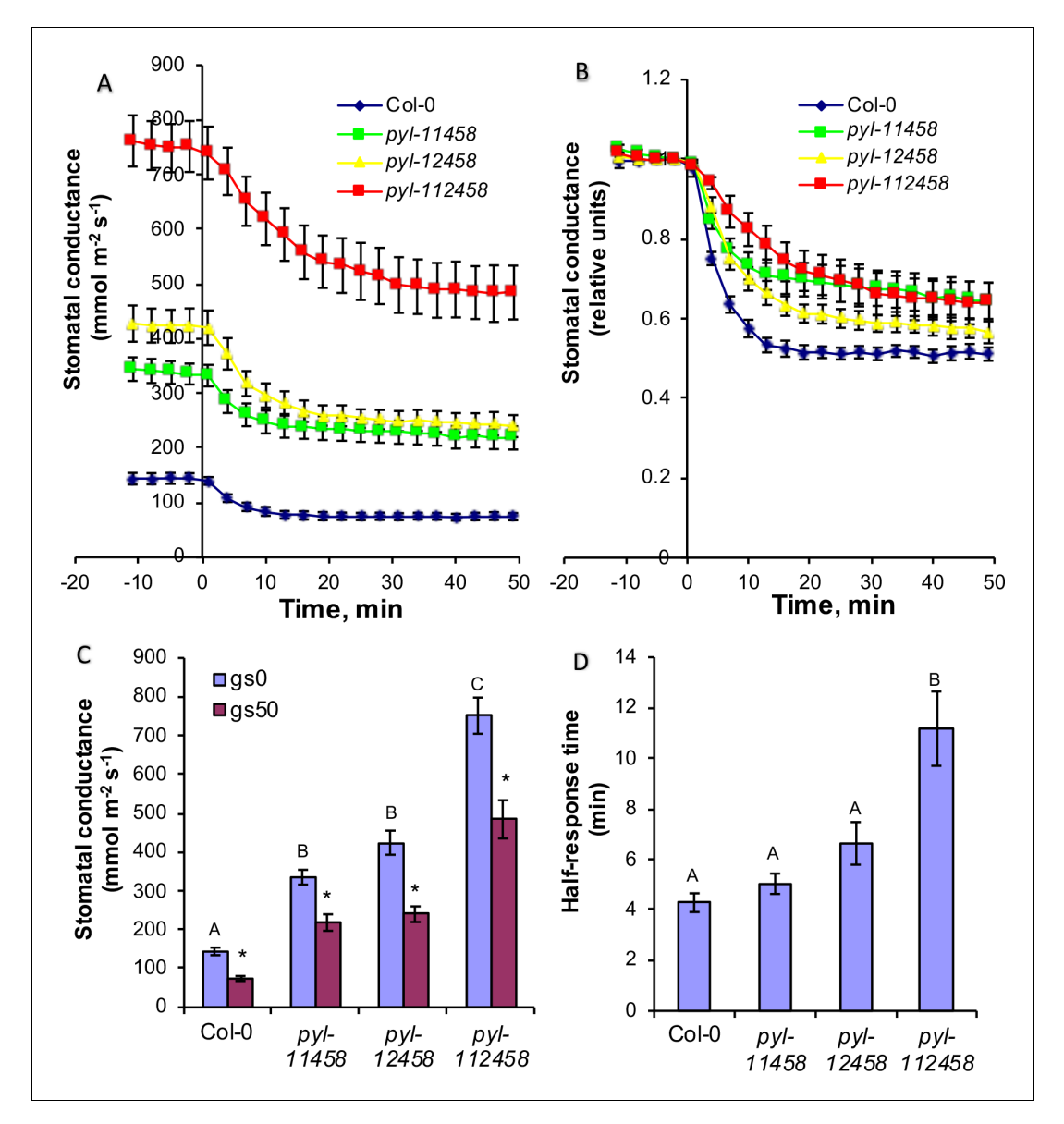


Figure 9. CO_2 elevation causes robust stomatal closing responses in two ABA receptor quintuple mutant and in ABA receptor sextuple mutant plants. (A, B) Time-resolved stomatal conductances of PYR/RCAR receptor quintuple (pyl-11458 and pyl-12458) and sextuple (pyl-112458) mutants. Air CO_2 concentration was increased from 400 ppm to 800 ppm at the zero timepoints. Gas exchange analyses are from n = 5 to 7 whole plants per genotype and condition, using methods described in *Merilo et al.*, 2018 (see Materials and methods). Data are presented in absolute (A) and relative (B) units. (C) Stomatal conductances before (gs0) and 50 min (gs50) after changing CO_2 from 400 ppm to 800 ppm, average and SE (n = 5 to 7 whole plants). Capital letters denote differences in gs0 (pre-treatment stomatal conductance) between the lines (n = 5 to 7 whole plants, ANOVA, p=0.000000), whereas stars denote whether gs50 is significantly different from gs0 of that line (n = 5 to 7 whole plants, ANOVA, p=0.00001). (D) Half-response times of stomatal closures in response to 50 min CO_2 enrichment. Capital letters denote significant differences between the lines (n = 5 to 7 whole plants, ANOVA, p=0.000023).

The online version of this article includes the following source data and figure supplement(s) for figure 9:

Source data 1. Stomatal conductance values of individual plants and half response times.

Figure supplement 1. PYR/RCAR ABA receptor pyr1 pyl2/4/5/8 quintuple mutant (pyl-12458) and pyr1 pyl1/2/4/5/8 (pyl-112458) sextuple mutant show larger absolute stomatal closing responses during the first 20 min under elevated CO_2 compared to wild-type (Col-0) (light blue bars).

Figure supplement 1—source data 1. Absolute and relative changes in stomatal conductance values used in Figure 9—figure supplement 1. Figure supplement 2. Stomata of ABA receptor quintuple mutant (pyr1/pyl1/pyl4/pyl5/pyl8) and guard cell-targeted (B) PYL1 and (C) PYL4 ABA receptor complemented plants show stomatal CO₂ responses similar to wild-type (Col-0) controls.

Figure supplement 2—source data 1. Stomatal conductance values of individual plants used in Figure 9—figure supplement 2. Figure supplement 3. Genotyping of ABA receptor multiple mutants and guard cell-targeted ABA receptor complemented plants.



SNACS (*Figure 1B*). The full length AKS1 protein functions as a transcription factor in the nucleus. However, the bHLH domain of AKS1, which is important for its transcription factor function and nuclear localization, was excluded from our SNACS sensor construct. SNACS fluorescence appears to be observed mainly in the cytoplasm and in cytoplasmic spaces between vacuoles, with possible weak or no expression in the nucleus (*Figure 3—figure supplement 1*). Future research can target SNACS to the nucleus or to other cellular compartments.

ABA caused relatively small SNACS FRET ratio shifts in guard cells. Blind ABA vs. EtOH control treatment experiments and controls with the mutant SNACS^{5785A} and *snrk2.2/2.3/2.6* triple mutant guard cells confirmed the ABA response of SNACS (*Figures 3, 4* and *5*). Protein kinase sensors for protein kinases have been developed that show small ratio shifts of 1% to 4% and have been used to address key biological questions (e.g. *Kajimoto et al., 2019*). In our study, the average response of SNACS to ABA was 3.7 ± 0.2% (n = 46 stomata,± SEM). The low background noise in these kinase sensors has enabled real-time analyses of kinase activation and inhibition (*Kajimoto et al., 2019*). Therefore, because of small ratio shifts, continuous recordings in individual cells are needed to resolve stimulus-dependent FRET changes (*Allen et al., 1999*), rather than investigating single time point comparisons of FRET ratios in different cells. FRET imaging with SNACS permits single cell-type imaging in real-time, compared to the need to purify very large numbers of cells and isolate extracts for each *in-gel* kinase assay lane.

The protein kinase inhibitor K252a, that is known to disrupt ABA signaling in guard cells (Schmidt et al., 1995), inhibits the ABA-induced FRET increase (Figure 6A). Furthermore, snrk2.2/ 2.3/2.6 triple mutants showed no clear ABA-induced FRET ratio shift (Figure 5D). These data suggest that the ABA-induced FRET ratio changes are dependent on protein phosphorylation (Figure 1C). Interestingly, we also found that K-252a induces a decrease of the SNACS FRET ratio when K252a was applied after the ABA-induced FRET ratio increase (Figure 6C). This would be consistent with a dephosphorylation of SNACS by a protein phosphatase in plant cells. We do not exclude the possibility that K252a affects another protein kinase activity, in addition to SnRK2 activities (Figure 6—figure supplement 1). The calmodulin inhibitor, that does not inhibit SnRK2.6/OST1 did not affect SNACS fluorescence ratios (Figure 6E; Figure 6—figure supplement 1). In ost1/ snrk2.6 single mutant guard cells and in snrk2.2/snrk2.3 double mutant guard cells, ABA caused increases in the FRET ratio of SNACS, but not in snrk2.2/2.3/2.6 triple mutant guard cells (Figure 5). Furthermore, SNACS-dependent FRET signals were reversed by protein kinase inhibitors (Figure 6). Together these data suggest that SNACS can report low baseline SnRK2 activity, and that SNACS can dynamically report biological changes in activity. HAB1 (also named AtP2C-HA) (Chérel et al., 2002; Saez et al., 2004; Leonhardt et al., 2004), a type 2C protein phosphatase involved in ABA signal transduction, does not appear to dephosphorylate the Ser-30 residue of the AKS1 transcription factor (Takahashi et al., 2017). PP2A phosphatases may dephosphorylate AKS1 (Bu et al., 2017). The K252a-induced reduction in the SNACS FRET ratio in guard cells provides evidence that the SNACS reporter is reversible. The potential reversibility of SNACS suggests that dynamic upand down-regulation of SnRK2 protein kinases can be investigated in intact plant cells in real-time.

Methyl jasmonate (MeJA) is a plant hormone that functions in many developmental processes and is important for plant defense responses (Melotto et al., 2017). However, MeJA appears to cause different regulation outcomes of stomata depending on conditions. MeJA-mediated stomatal closure was observed in several species including Paphiopedilum (Gehring, 1997), Vicia faba (Liu et al., 2002) and Arabidopsis (Suhita et al., 2004; Hossain et al., 2011; Munemasa et al., 2007; Munemasa et al., 2019; Yin et al., 2016; Förster et al., 2019). However, other studies reported that MeJA did not promote stomatal closure (Montillet et al., 2013; Savchenko et al., 2014; Melotto et al., 2017; Zhu et al., 2020). In addition, the SnRK2.6/OST1 protein kinase is required for MeJA-induced stomatal closure, due to an impaired MeJA-induced stomatal closure response in snrk2.6/ost1 mutants (Yin et al., 2016). Furthermore, in-gel kinase assays of guard cellenriched epidermal tissues suggest that MeJA does not activate SnRK2.6/OST1 activity even though OST1/SnRK2.6 mutation impairs MeJA-induced stomatal closing (Munemasa et al., 2019). In the present study, the SNACS reporter did not show clear increases in FRET ratios in guard cells upon 20 μM MeJA application, consistent with this study using guard cell-enriched epidermal tissues (Munemasa et al., 2019; Figure 7). These findings may support a recently proposed calcium-dependent parallel MeJA response pathway (Förster et al., 2019). The SNACS sensor reported here can be used to further investigate MeJA signaling under diverse conditions.



High CO₂ and ABA trigger rapid stomatal closure. Gas exchange, stomatal movement and ion channel regulation studies with ost1 mutant alleles demonstrated that the SnRK2.6/OST1 protein kinase plays a role in CO₂-induced stomatal closure (*Xue et al., 2011*; *Merilo et al., 2013*; *Hsu et al., 2018*). Surprisingly however, in-gel kinase assays suggested that CO₂ elevation did not enhance SnRK2.6/OST1 activity in guard cell protoplasts, even though high CO₂ activated S-type anion channels in the same system (*Hsu et al., 2018*). It remained unclear however whether elevated CO₂ can activate SnRK2 protein kinase activity in live intact guard cells. In the present study, we used the new SNACS reporter to investigate CO₂ signal transduction in intact stomatal guard cells. Time-resolved FRET analyses in guard cells show that CO₂ elevation does not cause measurable increases in the FRET ratio of SNACS-expressing guard cells, whereas subsequent exposure to ABA caused clear FRET ratio increases (*Figure 8A and B*), providing evidence in intact guard cells that high CO₂ does not activate the SnRK2.6/OST1 activity.

Studies have shown that ABA receptors and OST1/SnRK2.6 are required for wild-type like high CO₂-induced stomatal closure (Chater et al., 2015; Xue et al., 2011; Hsu et al., 2018). Classical studies suggested that non-stressed guard cells have a higher ABA concentration than other leaf cells (Lahr and Raschke, 1988) and more recently this has been shown experimentally (Hsu et al., 2018; Yoshida et al., 2019). A basal SnRK2 kinase activity was hypothesized in non-stressed guard cells to explain all experimental observations (Hsu et al., 2018). However, direct measurements of the basal SnRK2 activity in guard cells had not been possible. Interestingly, the protein kinase inhibitor K252a caused a clear decrease in FRET ratio of the SNACS reporter and K252a inhibited ABAinduced FRET changes of SNACS in guard cells (Figure 6A and D). Furthermore, the ABA-induced SNACS response is disrupted in the snrk2.2/2.3/2.6 triple mutant (Figure 5D). These data provide experimental evidence that SnRK2 protein kinases have a basal kinase activity in guard cells, even in the absence of exogenous ABA application. The basal SnRK2 activity found here could provide an explanation why ost1/snrk2.6 mutant alleles are clearly impaired in CO₂-induced stomatal closing (Xue et al., 2011; Hsu et al., 2018; Merilo et al., 2013), but elevated CO2 does not enhance OST1/ SnRK2.6 activity (Figure 8): The present data suggest that basal SnRK2 activity, functioning parallel to the CO₂ signal transduction branch, is required for and/or could amplify CO₂ signaling. Furthermore, high CO2-induced stomatal closing is slowed but not disrupted in ost1/snrk2.6 (Hsu et al., 2018). This lies in contrast to a stronger ABA-insensitive response of ost1/snrk2.6 mutant alleles (Mustilli et al., 2002; Yoshida et al., 2002). These findings are consistent with a parallel role for ABA and OST1 in CO₂ signal transduction.

A recent study has suggested that CO₂ signal transduction is mediated by the PYL4 and PYL5, but not the PYL2 ABA receptors (Dittrich et al., 2019). This conclusion could not be confirmed in the present study using higher order ABA receptor quintuple and sextuple mutant plants, that include gene disruptions of PYL4 and PYL5 (Figure 9, Figure 9-figure supplement 1, Figure 9figure supplement 2 and Figure 9-figure supplement 3). In the present study, quintuple ABA receptor disruption lines pyl-11458 and pyl-12458 were those investigated for gas exchange in Dittrich et al., 2019. However, data for the guard cell complementation lines presented here were based on pyl-11458 whereas gas exchange data in Dittrich et al., 2019 were based on complementation of pyl-12458. Protein expression levels of transgenically-expressed receptors may vary, affecting interpretations. Therefore, use of gene disruption lines in the present study allows for more reliable conclusions and demonstrates that CO₂-induced stomatal closing remains robust after PYL4 and PYL5 disruption (Figure 9 and Figure 9-figure supplement 1). Furthermore, quantitative differences in protein expression levels of transgenically-expressed ABA receptors in guard cells and growth conditions may affect the outcome of stomatal response data given the relevance of basal ABA concentrations and SnRK2 activity found here. The large transpiration rate in the pyl-12458 quintuple mutant was reduced by guard cell expression of PYL5 (Supplementary Figure 8C in Dittrich et al., 2019), which may be explained by the response to basal ABA. Consistent with this model, we observed a slowed stomatal opening in pyl-11458/PYL5 leaves (Figure 9—figure supplement 2D). Stomatal responses to high CO₂ were affected and slowed in higher order pyr/pyl/rcar ABA receptor mutants (Hsu et al., 2018). However, data for complementation with single receptors (Dittrich et al., 2019) may depend on growth conditions, as the present independent findings in our two laboratories (EM and HK lab and JS lab) and previous studies (Merilo et al., 2013; Hsu et al., 2018) could not support the model that PYL4 and PYL5 mediate the stomatal CO₂ response.



Normalization is often used to display stomatal responses of mutants with largely different steady-state stomatal conductances. Note that, apart from comparing the time dependence of stomatal responses, conclusions derived from interpretation of normalized stomatal conductance data can be equivocal. Mutants that respond to stimulation, but have a higher stomatal conductance and retain a higher stomatal conductance after the response (which may be due to stomatal development and apertures), can show an apparent reduced responsiveness when data are normalized to the values before the onset of a stimulus. As an example, in the present study analyses of normalized stomatal conductance data would lead to inaccurate conclusions: For example, when stomatal conductance data from Figure 9 were analyzed, but in normalized relative units, that is by dividing the absolute reduction in stomatal conductance with the stomatal conductance at the onset of elevated CO₂, the opposite conclusions to non-normalized data analyses could be made (Figure 9—figure supplement 1): After normalization the PYR/RCAR sextuple mutant and the pyl-11458 quintuple mutant had the smallest normalized reductions in stomatal conductance in response to CO2 elevation (Figure 9—figure supplement 1). In contrast however, for the same data, the absolute stomatal conductance values show the strongest CO₂ responses in the ABA receptor pyl-12458 guintuple and pyl-112458 sextuple mutants (Figure 9A and B, Figure 9—figure supplement 1). These analyses indicate that in order to quantitatively determine whether the stomata of plant lines with different initial stomatal conductances are sensitive to stimuli, it is necessary to apply various kinetic analysis based on non-normalized real-time stomatal conductances. Showing both absolute and normalized data side-by-side (Hsu et al., 2018), or providing steady-state stomatal conductance values, can help in developing more robust mechanistic models.

In conclusion, SnRK2s are key protein kinases that mediate abiotic stress responses. Together, the presented research provides a new approach to investigate real-time SnRK2 kinase activity and stress responses in living intact plant cells and tissues. The SNACS reporter could be used to investigate many stress signaling models, and cross talk among pathways (*Yoshida et al., 2006*; *Wang et al., 2018*; *Takahashi et al., 2020*; *Lin et al., 2020*). Furthermore, subcellular targeting of SNACS should be interesting for future comparisons of cellular compartment-localized SnRK2 protein kinase regulation. Furthermore, we provide evidence for the reversibility of SNACS in vivo upon inhibition of kinase activities, suggesting that SnRK2 protein kinase down-regulation can be analyzed as well. Moreover, both elevated CO₂ and MeJA did not cause SNACS fluorescence emission ratio increases, providing experimental evidence that these stimuli do not rapidly enhance SnRK2.6/OST1 activity in guard cells as found in real-time analyses here. Furthermore, our gas exchange analyses in intact plants and leaves, could not confirm the recently proposed model that stomatal CO₂ signaling requires the PYL4 and PYL5 ABA receptors (*Dittrich et al., 2019*). The present findings provide in vivo evidence for CO₂ signal transduction mechanisms in stomatal signaling that use basal ABA signaling and basal OST1 activity, but do not rapidly upregulate OST1/SnRK2 kinase activity.

Materials and methods

Key resources table

Reagent type (species) or resource	Designation	Source or reference	Identifiers	Additional information
Gene (Arabidopsis)	AKS1	Tair (https://www.arabidopsis.org/)	Tair ID: At1g51140	
Gene (Arabidopsis)	14-3-3, GF14phi	Tair (https://www.arabidopsis.org/)	Tair ID: At1g35160	
Strain, strain background (Escherichia coli)	BL21-CodonPlus (DE3)	Agilent Technologies Model: 230245		Electro- competent cells
Strain, strain background (Agrobacterium tumefaciens)	GV3101	Other		Widely distributed
Antibody	Anti-FLAG M2 Mouse monoclonal	Sigma-Aldrich	RRID:AB_262044	x5,000
Chemical compound, drug	K-252a	Sigma-Aldrich	Cas No. 99533-80-9	
Continued on next pag	je			



Continued

Reagent type (species) or resource	Designation	Source or reference	Identifiers	Additional information
Chemical compound, drug	W-7	Sigma-Aldrich	Cas No. 61714-27-0	
Chemical compound, drug	MeJA	Bedoukian Research, Inc	rch, Inc Ct. 06810–4192	
Software, algorithm	MetaFluor software	MetaFluor (https://www.moleculardevices. com/products/cellular-imaging- systems/acquisition-and-analysis- software/metamorph-microscopy)	RRID:SCR_014294	version 7.0r3
Software, algorithm	Fiji software	Fiji (https://imagej.net/Fiji)	RRID:SCR_002285	
Software, algorithm	GraphPad Prism software	GraphPad Prism (https://graphpad.com)	RRID:SCR_015807	version 7.0

Construction of SNACS reporter

The plasmid backbone used to construct SNACS reporter plasmids was the SOMA construct as reported by **Zaman et al., 2019**. Restriction enzyme cloning was used: the FHA domain in the original vector was replaced with the full-length 267 amino acid coding region of the 14-3-3 protein, GF14phi (At1g35160) and the substrate domain of the original plasmid was replaced with DNA encoding for amino acids 1–48 of the *Arabidopsis* AKS1 protein (At1g51140) (**Takahashi et al., 2017**). To generate the phospho-site mutant isoform of the SNACS reporter, site-directed mutagenesis was performed to change the coding sequence at the AKS1 serine-30 to alanine resulting in the SNACS^{5785A} reporter. In addition, the Strepll-tag was inserted into the C-terminus via the Xbal site for expression of recombinant SNACS protein in *E. coli*. For expression in plants, the SNACS coding fragment was PCR-amplified with the attB1 and attB2 adaptor primers. This fragment was introduced into the donor vector pDONR221 using BP clonase (Invitrogen). Final destination vectors for expression in plants were obtained by using a multisite gateway recombination system, using the pH7m34GW destination vector and p35S/pDONRP4-P1R constructs. Vectors carrying *35S: SNACS* or *35S: SNACS* were used for plant transformation.

In vitro FRET analyses and phosphorylation assay

The recombinant SNACS protein, SNACS^{S785A} protein, GST-OST1/SnRK2.6, GST-OST1^{D140A}, GST-CPK6 and GST-SnRK2.3 were expressed in BL21-CodonPlus (DE3)-RIL cells (Stratagene). StrepII-tagged proteins were purified using Strep-Tactin Macroprep columns (IBA). GST-tagged recombinant proteins were purified using Glutathione Sepharose 4B. 9 μ g of the SNACS or SNACS^{S785A} were added to a reaction containing 1 \times PKA buffer (50 mM Tris-HCl pH7.5, 10 mM MgCl₂), 0.2 mM ATP-Na, 2 mM DTT and water to a total volume of 50 μ l with 2 μ M free Ca²⁺ buffered only for GST-CPK6. For reactions including GST-OST1, GST-OST1^{D140A}, GST-CPK6, and GST-SnRK2.3, 4 μ g of these proteins were also added. The reactions were then incubated at room temperature for 2 hr and the fluorescence emission spectrum was measured using a TECAN SPARK multimode plate reader. Excitation was performed at 434 nm and the emission range analyzed was 460 to 560 nm.

In vitro phosphorylation assays were performed as previously described (*Takahashi et al., 2017*). Recombinant SNACS reporter proteins were incubated in phosphorylation buffer (50 mM Tris-HCl, 10 mM MgCl₂, 0.1% TritonX-100, 1 mM DTT, pH7.5) with recombinant GST-tagged OST1/SnRK2.6 or CPK6 for 30 min at room temperature in the presence of 1 μ Ci [γ -³²P]-ATP and 200 μ M ATP. The reactions were stopped by the addition of SDS-loading buffer. After separation with 10% SDS-polyacrylamide gels, proteins were visualized by coomassie blue staining, and phosphorylated proteins were visualized by autoradiography.

Infiltration of Nicotiana benthamiana for transient expression

SNACS driven by the CaMV 35S promoter was co-expressed with *pUBQ10:OST1-HF* via co-infiltration using the GV3101 strain of *Agrobacterium tumefaciens*. In parallel, we co-infiltrated *N. benthamiana* leaves using Agrobacterium carrying the p19 suppressor of gene silencing to enhance



transgene expression. *N. benthamiana* leaves from 3-week-old plants were used for infiltration. After 3 days of infiltration, microscope imaging analyses were performed (see below).

Transgenic Arabidopsis lines and plant growth

SNACS and SNACS^{5785A} reporters carrying plasmids were transformed into the *Arabidopsis* Columbia 0 accession expressing, pUBQ10:OST1-HF in the ost1-3 genetic background (*Waadt et al.*, 2015), ost1-3 (salk_008068) (*Yoshida et al.*, 2002), snrk2.2/2.3 (GABI-Kat_807G04/salk_107315) and snrk2.2/3/6 (GABI-Kat_807G04/salk_107315/salk_008068) (*Brandt et al.*, 2015) via the floral dip method using the GV3101 strain of *Agrobacterium tumefaciens* (*Zhang et al.*, 2006). Primary transformants expressing the sensor constructs were selected on 0.5 MS supplemented with 25 μ g/mL hygromycin and further cultivated in soil in a growth room (16 h day/8 hr night). We selected positive transformants by fluorescence intensity using confocal microscopy as described below. Transgenic *Arabidopsis* lines used in the present study are listed in *Supplementary file* 1.

Sample preparation and imaging analyses

For N. benthamiana and Arabidopsis imaging, detached N. benthamiana and Arabidopsis leaves were prepared with the abaxial leaf epidermises on a cover glass using medical adhesive (Holliser, Libertyville, IL). A razor blade was then used to carefully remove the upper mesophyll cell layers of N. benthamiana and Arabidopsis leaves to yield intact epidermal strips (Young et al., 2006), which were further incubated in 2 mL assay buffer (5 mM KCl, 50 μM CaCl₂, 10 mM MES-Tris, pH 5.6) for an additional 1 hr. 4- to 6- week-old transgenic Arabidopsis plants were used. FRET ratio-imaging was conducted as previously described (Waadt et al., 2014; Allen et al., 1999), with the difference of using 150 ms exposures to reduce bleaching of the fluorescent proteins. Ratiometric measurements were conducted by interchanging the following band-pass emission filters 480 nm (DF30) and 535 nm (DF25) with a computer-controlled filter wheel (Allen et al., 1999). Excitation light was 434 nm (DF20) (Allen et al., 1999). Images were acquired in intervals of 6 s using MetaFluor software. Image analyses and processing were conducted using Fiji with the following applications: Background subtraction, gaussian blur, 32-bit conversion, threshold, ratio calculation and physics look up (Schindelin et al., 2012). Whole individual stomata including the central stomatal pore were selected as regions of interest (ROI) for individual stomate ratio imaging using Fiji and the average ratio value within that ROI was then measured. For background subtraction, epidermal pavement cell background regions were analyzed in which no evident fluorescence of the SNACS reporter was evident. The fluorescence intensity of the SNACS reporter in guard cells appeared to be higher than that in epidermal pavement cells or the SNACS expression levels in the cytoplasm of quard cells appeared to be higher than in surrounding cells. Note that the focal plane during imaging in the present study was focused on guard cells, which is slightly shifted from the focal plane of epidermal pavement cells (Figure 2—figure supplement 1). Additionally, since we investigated SNACS-dependent FRET responses in stomata in the present study, we choose microscopic regions in some experiments showing SNACS fluorescence in guard cells with apparent low SNACS fluorescence in surrounding epidermal cells. Therefore, at the illustrated image gains, epidermal cells are not clearly visible. The FRET ratio of YPet to Turquoise GL emission fluorescence was normalized to the average over first 5 min before the indicated treatments. For the indicated treatment applications, epidermal strips were perfused by gently pipetting 5 to 6 times with the assay buffer supplemented with the indicated final concentrations of treatment (ABA, K252a, W-7, MeJA and solvent controls). CO₂ responses of the SNACS reporter were performed as previously described (Hsu et al., 2018) except that solutions for high CO₂ were bubbled with air containing 2000 ppm CO₂. The final CO₂ concentrations in the recording chamber of 115 ppm and 1170 ppm after bath perfusion from continuously bubbled solutions to the imaging chamber via tubing and a peristaltic pump were determined as described previously (Young et al., 2006). For ABAleon2.15 reporter imaging, experiments were performed as described above, except that images were acquired in intervals of 12 s. The FRET ratio of YPet to Turquoise GL emission fluorescence was normalized to the average over the first 10 min for CO₂ response experiments. Paired t-test analyses were performed using Graphpad Prism version 7.0.



Whole plant gas exchange experiments

25-30 days old Arabidopsis plants grown in pots containing 2:1 (v:v) peat: vermiculite mixture kept in Snijders chambers (Snijders Scientific, Drogenbos, Belgia) at 12/12 photoperiod, 23/18 °C temperature, 160 μ mol m⁻² s⁻¹ light and 70% relative humidity, were used for gas exchange experiments. Custom-built 8-chamber temperature-controlled gas-exchange device as described before (Kollist et al., 2007) was used to measure water vapor concentrations in the air entering and leaving the measurement chambers and to calculate the values of whole-plant stomatal conductance. Standard conditions during the 1-2 hr stabilization period were: ambient CO₂ (~400 ppm), light 160 μ mol m⁻² s⁻¹, relative air humidity (RH) ~61 ± 3%. Then, the CO₂ concentration was increased to 800 ppm for 50 min. Plant area was calculated from photographs using ImageJ 1.37 v (National Institutes of Health, USA). Stomatal conductance to water vapor is calculated as described in von Caemmerer and Farquhar, 1981, with details of the calculation procedure having been described earlier (Kollist et al., 2007). In order to compare the CO2 responses of different lines, we calculated closure half-times and rapid high CO2-induced changes in stomatal conductance. The whole 50 min stomatal response was scaled to a range of 0-100% and the time when 50% of stomatal closure was reached was calculated for half-response times. Rapid high CO₂-induced changes in stomatal conductance were calculated as the differences in the values of stomatal conductance 20 min after elevated CO₂ was applied and pretreatment stomatal conductance values.

Time-Resolved intact leaf stomatal conductance experiments

ABA receptor quintuple mutant, *pyr1/pyl1/pyl4/pyl5/pyl8* (**Antoni et al., 2013**), and guard cell-targeted ABA receptor complemented plants, *pyr1/pyl1/pyl4/pyl5/pyl8/pGC1::PYL1* (*pyl-11458/PYL1*), *pyr1/pyl1/pyl4/pyl5/pyl8/pGC1::PYL4* (*pyl-11458/PYL4*), and *pyr1/pyl1/pyl4/pyl5/pyl8/pGC1::PYL5* (*pyl-11458/PYL5*) were used for gas exchange analyses (**Antoni et al., 2013**; **Dittrich et al., 2019**). Stomatal conductance recordings from intact leaves of 5- to 6.5-week-old plants were conducted starting 1 to 2 hr after growth chamber light onset. A Li-6400XT infrared (IRGA)-based gas exchange analyzer system was used with an integrated 6400-02B LED Light Source (Li-Cor Inc). The measurement protocols were similar to those described by **Dittrich et al., 2019**. Leaves were clamped and kept in the dark at 400 ppm ambient CO₂ (**Dittrich et al., 2019**), 21°C, 65–70% relative air humidity, and 400 μmol s⁻¹ flow rate until the stomatal conductance stabilized. For stomatal responses to light and [CO₂] shifts, stomatal conductance was first measured at 400 ppm ambient CO₂ in the dark for 10 mins; then exposed to continuous light intensity 125 μmol m⁻² s⁻¹ (**Dittrich et al., 2019**). Approximately 80 mins after light-on, ambient [CO₂] was increased to 1000 ppm (**Dittrich et al., 2019**) to analyze stomatal responses to high [CO₂]. Following gas exchange experiments, the area of each analyzed leaf was measured for stomatal conductance calculations.

Higher order ABA receptor mutants in the present study were genotyped (*Figure 9—figure supplement 3*). Because the guard cell-targeted ABA receptor complementation lines were segregating (*Dittrich et al., 2019*), the *pGC1::PYL1*, *pGC1::PYL4*, and *pGC1::PYL5* transgene in each plant analyzed by gas exchange was subsequently confirmed by PCR in the present study (*Figure 9—figure supplement 3*). We have also isolated homozygous *pyr1/pyl1/pyl4/pyl5/pyl8/pGC1::PYL1*, *pyr1/pyl1/pyl4/pyl5/pyl8/pGC1::PYL4*, and *pyr1/pyl1/pyl4/pyl5/pyl8/pGC1::PYL5* lines. The seeds of the homozygous higher order ABA receptor mutants and homozygous guard cell-targeted ABA receptor complementation lines used in this study will be donated to the Arabidopsis Biological Resource Center.

Acknowledgements

We thank Dr. Alexandra Newton for discussions, Dr. Rainer Waadt for general advice on FRET imaging and Dr. Pedro L Rodriguez for providing the original ABA receptor mutant seeds. This research was funded by grants from the National Institutes of Health (GM060396) and the National Science Foundation to JIS (MCB-1900567). LZ was supported by a China Scholarship Council fellowship, and YT was supported by a Postdoctoral Fellowship for Research Abroad from the Japan Society for the Promotion of Science. Data of EM and HK in *Figure 9* and *Figure 9—figure supplements 1* and 2 were supported by the Estonian Research Council (grants PUT1133, PRG719 and PRG433) and



European Regional Development Fund (Center of Excellence in Molecular Cell Engineering CEMCE). PK was supported by the National Science Foundation (NSF MCB-1137950).

Additional information

Funding

Funder	Grant reference number	Author
National Science Foundation	MCB-1900567	Julian I Schroeder
National Institutes of Health	GM060396	Julian I Schroeder
China Scholarship Council		Li Zhang
Japan Society for the Promotion of Science		Yohei Takahashi
Eesti Teadusagentuur	PUT1133	Ebe Merilo
Eesti Teadusagentuur	PRG719	Ebe Merilo
Eesti Teadusagentuur	PRG433	Hannes Kollist
European Regional Develop- ment Fund	Center of Excellence in Molecular Cell Engineering (CEMCE)	Hannes Kollist
National Science Foundation	MCB-1137950	Patrick J Krysan

The funders had no role in study design, data collection and interpretation, or the decision to submit the work for publication.

Author contributions

Li Zhang, Investigation, Writing - original draft; Yohei Takahashi, Conceptualization, Investigation, Methodology, Writing - original draft, Writing - review and editing; Po-Kai Hsu, Hannes Kollist, Ebe Merilo, Investigation, Methodology, Writing - original draft, Writing - review and editing; Patrick J Krysan, Methodology, Writing - review and editing; Julian I Schroeder, Supervision, Funding acquisition, Methodology, Writing - original draft, Project administration, Writing - review and editing

Author ORCIDs

Li Zhang (b) https://orcid.org/0000-0003-0467-0290

Yohei Takahashi https://orcid.org/0000-0002-9406-4093

Po-Kai Hsu (b) https://orcid.org/0000-0001-7265-7077

Julian I Schroeder (b) https://orcid.org/0000-0002-3283-5972

Decision letter and Author response

Decision letter https://doi.org/10.7554/eLife.56351.sa1 Author response https://doi.org/10.7554/eLife.56351.sa2

Additional files

Supplementary files

- Supplementary file 1. Transgenic lines used in this study. Detailed information on the transgenic lines is provided including the plasmid, promoter, and genetic background.
- Supplementary file 2. Primer sequences for genotyping. Primers used to genotype higher order ABA receptor mutants (*Figure 9—figure supplement 3*).
- Transparent reporting form

Data availability

Data generated or analysed during this study are included in the manuscript and supporting files.



References

- Akter N, Sobahan MA, Uraji M, Ye W, Hossain MA, Mori IC, Nakamura Y, Murata Y. 2012. Effects of depletion of glutathione on abscisic acid- and methyl jasmonate-induced stomatal closure in *Arabidopsis thaliana*. Bioscience, Biotechnology, and Biochemistry **76**:2032–2037. DOI: https://doi.org/10.1271/bbb.120384, PMID: 23132563
- Allen GJ, Kwak JM, Chu SP, Llopis J, Tsien RY, Harper JF, Schroeder JI. 1999. Cameleon calcium Indicator reports cytoplasmic calcium dynamics in *Arabidopsis* guard cells. *The Plant Journal* 19:735–747. DOI: https://doi.org/10.1046/j.1365-313x.1999.00574.x, PMID: 10571859
- Antoni R, Gonzalez-Guzman M, Rodriguez L, Peirats-Llobet M, Pizzio GA, Fernandez MA, De Winne N, De Jaeger G, Dietrich D, Bennett MJ, Rodriguez PL. 2013. PYRABACTIN RESISTANCE1-LIKE8 plays an important role for the regulation of abscisic acid signaling in root. *Plant Physiology* **161**:931–941. DOI: https://doi.org/10.1104/pp.112.208678, PMID: 23370718
- Aoki K, Komatsu N, Hirata E, Kamioka Y, Matsuda M. 2012. Stable expression of FRET biosensors: a new light in Cancer research. Cancer Science 103:614–619. DOI: https://doi.org/10.1111/j.1349-7006.2011.02196.x, PMID: 22188216
- Ardito F, Giuliani M, Perrone D, Troiano G, Lo Muzio L. 2017. The crucial role of protein phosphorylation in cell signaling and its use as targeted therapy (Review). *International Journal of Molecular Medicine* 40:271–280. DOI: https://doi.org/10.3892/ijmm.2017.3036, PMID: 28656226
- Boudsocq M, Laurière C. 2005. Osmotic signaling in plants: multiple pathways mediated by emerging kinase families. Plant Physiology 138:1185–1194. DOI: https://doi.org/10.1104/pp.105.061275, PMID: 16009994
- Brandt B, Brodsky DE, Xue S, Negi J, Iba K, Kangasjärvi J, Ghassemian M, Stephan AB, Hu H, Schroeder JI. 2012.
 Reconstitution of abscisic acid activation of SLAC1 anion channel by CPK6 and OST1 kinases and branched
 ABI1 PP2C phosphatase action. PNAS 109:10593–10598. DOI: https://doi.org/10.1073/pnas.1116590109,
 PMID: 22689970
- Brandt B, Munemasa S, Wang C, Nguyen D, Yong T, Yang PG, Poretsky E, Belknap TF, Waadt R, Alemán F, Schroeder JI. 2015. Calcium specificity signaling mechanisms in abscisic acid signal transduction in *Arabidopsis* guard cells. *eLife* **4**:e03599. DOI: https://doi.org/10.7554/eLife.03599
- **Bu SL**, Liu C, Liu N, Zhao JL, Ai LF, Chi H, Li KL, Chien CW, Burlingame AL, Zhang SW, Wang ZY. 2017. Immunopurification and mass spectrometry identifies protein phosphatase 2A (PP2A) and BIN2/GSK3 as regulators of AKS transcription factors in *Arabidopsis*. *Molecular Plant* **10**:345–348. DOI: https://doi.org/10.1016/j.molp.2016.09.016, PMID: 27769939
- Chater C, Peng K, Movahedi M, Dunn JA, Walker HJ, Liang YK, McLachlan DH, Casson S, Isner JC, Wilson I, Neill SJ, Hedrich R, Gray JE, Hetherington AM. 2015. Elevated CO2-Induced responses in stomata require ABA and ABA signaling. Current Biology 25:2709–2716. DOI: https://doi.org/10.1016/j.cub.2015.09.013, PMID: 26455301
- Chérel I, Michard E, Platet N, Mouline K, Alcon C, Sentenac H, Thibaud JB. 2002. Physical and functional interaction of the *Arabidopsis* K⁽⁺⁾ channel AKT2 and phosphatase AtPP2CA. *The Plant Cell* **14**:1133–1146. DOI: https://doi.org/10.1105/tpc.000943, PMID: 12034902
- Cutler SR, Rodriguez PL, Finkelstein RR, Abrams SR. 2010. Abscisic acid: emergence of a core signaling network. Annual Review of Plant Biology 61:651–679. DOI: https://doi.org/10.1146/annurev-arplant-042809-112122, PMID: 20192755
- Day RN, Davidson MW. 2009. The fluorescent protein palette: tools for cellular imaging. *Chemical Society Reviews* **38**:2887–2921. DOI: https://doi.org/10.1039/b901966a, PMID: 19771335
- Dittrich M, Mueller HM, Bauer H, Peirats-Llobet M, Rodriguez PL, Geilfus CM, Carpentier SC, Al Rasheid KAS, Kollist H, Merilo E, Herrmann J, Müller T, Ache P, Hetherington AM, Hedrich R. 2019. The role of *Arabidopsis* ABA receptors from the PYR/PYL/RCAR family in stomatal acclimation and closure signal integration. *Nature Plants* 5:1002–1011. DOI: https://doi.org/10.1038/s41477-019-0490-0, PMID: 31451795
- Förster S, Schmidt LK, Kopic E, Anschütz Ü, Huang S, Schlücking K, Köster P, Waadt R, Larrieu A, Batistič O, Rodriguez PL, Grill E, Kudla J, Becker D. 2019. Wounding-Induced stomatal closure requires Jasmonate-Mediated activation of GORK K⁺Channels by a Ca²⁺Sensor-Kinase CBL1-CIPK5 Complex. *Developmental Cell* **48**:87–99. DOI: https://doi.org/10.1016/j.devcel.2018.11.014, PMID: 30528785
- Fujii H, Verslues PE, Zhu JK. 2007. Identification of two protein kinases required for abscisic acid regulation of seed germination, root growth, and gene expression in *Arabidopsis*. The Plant Cell 19:485–494. DOI: https://doi.org/10.1105/tpc.106.048538, PMID: 17307925
- Fujii H, Zhu JK. 2009. Arabidopsis mutant deficient in 3 abscisic acid-activated protein kinases reveals critical roles in growth, reproduction, and stress. PNAS 106:8380–8385. DOI: https://doi.org/10.1073/pnas. 0903144106, PMID: 19420218
- Fujita Y, Nakashima K, Yoshida T, Katagiri T, Kidokoro S, Kanamori N, Umezawa T, Fujita M, Maruyama K, Ishiyama K, Kobayashi M, Nakasone S, Yamada K, Ito T, Shinozaki K, Yamaguchi-Shinozaki K. 2009. Three SnRK2 protein kinases are the main positive regulators of abscisic acid signaling in response to water stress in Arabidopsis. Plant and Cell Physiology 50:2123–2132. DOI: https://doi.org/10.1093/pcp/pcp147, PMID: 1 9880399
- Furihata T, Maruyama K, Fujita Y, Umezawa T, Yoshida R, Shinozaki K, Yamaguchi-Shinozaki K. 2006. Abscisic acid-dependent multisite phosphorylation regulates the activity of a transcription activator AREB1. PNAS 103: 1988–1993. DOI: https://doi.org/10.1073/pnas.0505667103, PMID: 16446457



- Gao X, Zhang J. 2008. Spatiotemporal analysis of differential akt regulation in plasma membrane microdomains. Molecular Biology of the Cell 19:4366–4373. DOI: https://doi.org/10.1091/mbc.e08-05-0449, PMID: 18701703
 Gehring C. 1997. Jasmonates induce intracellular alkalinization and closure of Paphiopedilum Guard cells. Annals of Botany 80:485–489. DOI: https://doi.org/10.1006/anbo.1997.0471
- Geiger D, Scherzer S, Mumm P, Stange A, Marten I, Bauer H, Ache P, Matschi S, Liese A, Al-Rasheid KA, Romeis T, Hedrich R. 2009. Activity of guard cell anion channel SLAC1 is controlled by drought-stress signaling kinase-phosphatase pair. PNAS 106:21425–21430. DOI: https://doi.org/10.1073/pnas.0912021106, PMID: 19955405
- Gonzalez-Guzman M, Pizzio GA, Antoni R, Vera-Sirera F, Merilo E, Bassel GW, Fernández MA, Holdsworth MJ, Perez-Amador MA, Kollist H, Rodriguez PL. 2012. *Arabidopsis* PYR/PYL/RCAR receptors play a major role in quantitative regulation of stomatal aperture and transcriptional response to abscisic acid. *The Plant Cell* 24: 2483–2496. DOI: https://doi.org/10.1105/tpc.112.098574, PMID: 22739828
- Herde O, Pena-Cortes H. 1997. Stomatal responses to jasmonic acid, linolenic acid and abscisic acid in wild-type and ABA-deficient tomato plants. Plant and Cell Environment 141:11. DOI: https://doi.org/10.1046/j.1365-3040.1997.d01-11.x
- Hossain MA, Munemasa S, Uraji M, Nakamura Y, Mori IC, Murata Y. 2011. Involvement of endogenous abscisic acid in methyl jasmonate-induced stomatal closure in *Arabidopsis*. *Plant Physiology* **156**:430–438. DOI: https://doi.org/10.1104/pp.111.172254, PMID: 21402795
- Hrabak EM, Chan CW, Gribskov M, Harper JF, Choi JH, Halford N, Kudla J, Luan S, Nimmo HG, Sussman MR, Thomas M, Walker-Simmons K, Zhu JK, Harmon AC. 2003. The Arabidopsis CDPK-SnRK superfamily of protein kinases. Plant Physiology 132:666–680. DOI: https://doi.org/10.1104/pp.102.011999, PMID: 12805596
- Hsu PK, Takahashi Y, Munemasa S, Merilo E, Laanemets K, Waadt R, Pater D, Kollist H, Schroeder JI. 2018. Abscisic acid-independent stomatal CO₂ signal transduction pathway and convergence of CO₂ and ABA signaling downstream of OST1 kinase. *PNAS* 115:E9971–E9980. DOI: https://doi.org/10.1073/pnas. 1809204115, PMID: 30282744
- Jones AM, Grossmann G, Danielson JÅ, Sosso D, Chen LQ, Ho CH, Frommer WB. 2013. *In vivo* biochemistry: applications for small molecule biosensors in plant biology. *Current Opinion in Plant Biology* **16**:389–395. DOI: https://doi.org/10.1016/j.pbi.2013.02.010, PMID: 23587939
- Kajimoto T, Caliman AD, Tobias IS, Okada T, Pilo CA, Van AN, Andrew McCammon J, Nakamura SI, Newton AC. 2019. Activation of atypical protein kinase C by sphingosine 1-phosphate revealed by an aPKC-specific activity reporter. Science Signaling 12:eaat6662. DOI: https://doi.org/10.1126/scisignal.aat6662, PMID: 30600259
- Kobayashi Y, Yamamoto S, Minami H, Kagaya Y, Hattori T. 2004. Differential activation of the rice sucrose nonfermenting1-related protein kinase2 family by hyperosmotic stress and abscisic acid. *The Plant Cell* 16: 1163–1177. DOI: https://doi.org/10.1105/tpc.019943, PMID: 15084714
- Kollist T, Moldau H, Rasulov B, Oja V, Rämma H, Hüve K, Jaspers P, Kangasjärvi J, Kollist H. 2007. A novel device detects a rapid ozone-induced transient stomatal closure in intact Arabidopsis and its absence in abi2 mutant. Physiologia Plantarum 129:796–803. DOI: https://doi.org/10.1111/j.1399-3054.2006.00851.x
- Lahr W, Raschke K. 1988. Abscisic-acid contents and concentrations in protoplasts from guard cells and mesophyll cells of Vicia faba L. Planta 173:528–531. DOI: https://doi.org/10.1007/BF00958966, PMID: 24226690
- Lee SC, Lan W, Buchanan BB, Luan S. 2009. A protein kinase-phosphatase pair interacts with an ion channel to regulate ABA signaling in plant guard cells. *PNAS* 106:21419–21424. DOI: https://doi.org/10.1073/pnas. 0910601106, PMID: 19955427
- Leonhardt N, Kwak JM, Robert N, Waner D, Leonhardt G, Schroeder JI. 2004. Microarray expression analyses of Arabidopsis guard cells and isolation of a recessive abscisic acid hypersensitive protein phosphatase 2C mutant. The Plant Cell 16:596–615. DOI: https://doi.org/10.1105/tpc.019000, PMID: 14973164
- Li J, Wang XQ, Watson MB, Assmann SM. 2000. Regulation of abscisic acid-induced stomatal closure and anion channels by guard cell AAPK kinase. *Science* 287:300–303. DOI: https://doi.org/10.1126/science.287.5451.300, PMID: 10634783
- Li J, Assmann SM. 1996. An abscisic Acid-Activated and Calcium-Independent protein kinase from guard cells of fava bean. The Plant Cell 8:2359–2368. DOI: https://doi.org/10.2307/3870474, PMID: 12239380
- Lin W, Mehta S, Zhang J. 2019. Genetically encoded fluorescent biosensors illuminate kinase signaling in Cancer. Journal of Biological Chemistry 294:14814–14822. DOI: https://doi.org/10.1074/jbc.REV119.006177, PMID: 31434714
- Lin Z, Li Y, Zhang Z, Liu X, Hsu C-C, Du Y, Sang T, Zhu C, Wang Y, Satheesh V, Pratibha P, Zhao Y, Song C-P, Tao WA, Zhu J-K, Wang P. 2020. A RAF-SnRK2 kinase cascade mediates early osmotic stress signaling in higher plants. *Nature Communications* 11:1–10. DOI: https://doi.org/10.1038/s41467-020-14477-9
- Liu X, Zhang S, Lou C, Yv F. 2002. Effect of localized scorch on the transport and distribution of exogenous jasmonic acid in *Vicia faba*. Acta Botanica Sinica 44:164–167.
- Manning G, Whyte DB, Martinez R, Hunter T, Sudarsanam S. 2002. The protein kinase complement of the human genome. Science 298:1912–1934. DOI: https://doi.org/10.1126/science.1075762, PMID: 12471243
- Melotto M, Zhang L, Oblessuc PR, He SY. 2017. Stomatal defense a decade later. *Plant Physiology* **174**:561–571. DOI: https://doi.org/10.1104/pp.16.01853, PMID: 28341769
- Merilo E, Laanemets K, Hu H, Xue S, Jakobson L, Tulva I, Gonzalez-Guzman M, Rodriguez PL, Schroeder JI, Broschè M, Kollist H. 2013. PYR/RCAR receptors contribute to ozone-, reduced air humidity-, darkness-, and CO₂-induced stomatal regulation. *Plant Physiology* **162**:1652–1668. DOI: https://doi.org/10.1104/pp.113. 220608, PMID: 23703845



- Merilo E, Yarmolinsky D, Jalakas P, Parik H, Tulva I, Rasulov B, Kilk K, Kollist H. 2018. Stomatal VPD response: there is more to the story than ABA. *Plant Physiology* **176**:851–864. DOI: https://doi.org/10.1104/pp.17.00912, PMID: 28986421
- Miyawaki A, Tsien RY. 2000. Monitoring protein conformations and interactions by fluorescence resonance energy transfer between mutants of green fluorescent protein. *Methods in Enzymology* **327**:472–500. DOI: https://doi.org/10.1016/s0076-6879(00)27297-2, PMID: 11045004
- Montillet JL, Leonhardt N, Mondy S, Tranchimand S, Rumeau D, Boudsocq M, Garcia AV, Douki T, Bigeard J, Laurière C, Chevalier A, Castresana C, Hirt H. 2013. An abscisic acid-independent oxylipin pathway controls stomatal closure and immune defense in *Arabidopsis*. *PLOS Biology* **11**:e1001513. DOI: https://doi.org/10.1371/journal.pbio.1001513, PMID: 23526882
- Mori IC, Muto S. 1997. Abscisic acid activates a 48-Kilodalton protein kinase in guard cell protoplasts. *Plant Physiology* **113**:833–839. DOI: https://doi.org/10.1104/pp.113.3.833, PMID: 12223647
- Munemasa S, Oda K, Watanabe-Sugimoto M, Nakamura Y, Shimoishi Y, Murata Y. 2007. The coronatine-insensitive 1 mutation reveals the hormonal signaling interaction between abscisic acid and methyl jasmonate in *Arabidopsis* guard cells. specific impairment of ion channel activation and second messenger production. *Plant Physiology* **143**:1398–1407. DOI: https://doi.org/10.1104/pp.106.091298, PMID: 17220365
- Munemasa S, Hirao Y, Tanami K, Mimata Y, Nakamura Y, Murata Y. 2019. Ethylene inhibits methyl Jasmonate-Induced stomatal closure by modulating guard cell Slow-Type anion channel activity via the OPEN STOMATA 1/SnRK2.6 Kinase-Independent Pathway in *Arabidopsis*. *Plant and Cell Physiology* 60:2263–2271. DOI: https://doi.org/10.1093/pcp/pcz121, PMID: 31241163
- Mustilli AC, Merlot S, Vavasseur A, Fenzi F, Giraudat J. 2002. Arabidopsis OST1 protein kinase mediates the regulation of stomatal aperture by abscisic acid and acts upstream of reactive oxygen species production. The Plant Cell 14:3089–3099. DOI: https://doi.org/10.1105/tpc.007906, PMID: 12468729
- Nakashima K, Fujita Y, Kanamori N, Katagiri T, Umezawa T, Kidokoro S, Maruyama K, Yoshida T, Ishiyama K, Kobayashi M, Shinozaki K, Yamaguchi-Shinozaki K. 2009. Three *Arabidopsis* SnRK2 protein kinases, SRK2D/SnRK2.2, SRK2E/SnRK2.6/OST1 and SRK2I/SnRK2.3, involved in ABA signaling are essential for the control of seed development and dormancy. *Plant and Cell Physiology* **50**:1345–1363. DOI: https://doi.org/10.1093/pcp/pcp083, PMID: 19541597
- Raghavendra AS, Gonugunta VK, Christmann A, Grill E. 2010. ABA perception and signalling. Trends in Plant Science 15:395–401. DOI: https://doi.org/10.1016/j.tplants.2010.04.006, PMID: 20493758
- Raschke K. 1975. Simultaneous requirement of carbon dioxide and abscisic acid for stomatal closing in Xanthium strumarium L. Planta 125:243–259. DOI: https://doi.org/10.1007/BF00385601, PMID: 24435438
- Raschke K, Pierce M, Popiela CC. 1976. Abscisic acid content and stomatal sensitivity to CO(2) in leaves of Xanthium strumarium L. after pretreatments in warm and cold growth chambers. Plant Physiology **57**:115–121. DOI: https://doi.org/10.1104/pp.57.1.115, PMID: 16659416
- Rudd JJ, Franklin F, Lord JM, Franklin-Tong VE. 1996. Increased phosphorylation of a 26-kD pollen protein is induced by the Self-Incompatibility response in *Papaver rhoeas*. The Plant Cell **8**:713–724. DOI: https://doi.org/10.1105/tpc.8.4.713, PMID: 12239397
- Saez A, Apostolova N, Gonzalez-Guzman M, Gonzalez-Garcia MP, Nicolas C, Lorenzo O, Rodriguez PL. 2004. Gain-of-function and loss-of-function phenotypes of the protein phosphatase 2C HAB1 reveal its role as a negative regulator of abscisic acid signalling. The Plant Journal 37:354–369. DOI: https://doi.org/10.1046/j. 1365-313X.2003.01966.x, PMID: 14731256
- Sample V, Mehta S, Zhang J. 2014. Genetically encoded molecular probes to visualize and perturb signaling dynamics in living biological systems. *Journal of Cell Science* 127:1151–1160. DOI: https://doi.org/10.1242/jcs. 099994, PMID: 24634506
- Savchenko T, Kolla VA, Wang CQ, Nasafi Z, Hicks DR, Phadungchob B, Chehab WE, Brandizzi F, Froehlich J, Dehesh K. 2014. Functional convergence of oxylipin and abscisic acid pathways controls stomatal closure in response to drought. *Plant Physiology* 164:1151–1160. DOI: https://doi.org/10.1104/pp.113.234310, PMID: 24429214
- Schindelin J, Arganda-Carreras I, Frise E, Kaynig V, Longair M, Pietzsch T, Preibisch S, Rueden C, Saalfeld S, Schmid B, Tinevez JY, White DJ, Hartenstein V, Eliceiri K, Tomancak P, Cardona A. 2012. Fiji: an open-source platform for biological-image analysis. *Nature Methods* 9:676–682. DOI: https://doi.org/10.1038/nmeth.2019, PMID: 22743772
- Schmidt C, Schelle I, Liao YJ, Schroeder JI. 1995. Strong regulation of slow anion channels and abscisic acid signaling in guard cells by phosphorylation and dephosphorylation events. PNAS 92:9535–9539. DOI: https://doi.org/10.1073/pnas.92.21.9535, PMID: 11607582
- Sluchanko NN, Beelen S, Kulikova AA, Weeks SD, Antson AA, Gusev NB, Strelkov SV. 2017. Structural basis for the interaction of a human small heat shock protein with the 14-3-3 universal signaling regulator. Structure 25: 305–316. DOI: https://doi.org/10.1016/j.str.2016.12.005, PMID: 28089448
- Stone JM, Walker JC. 1995. Plant protein kinase families and signal transduction. *Plant Physiology* **108**:451–457. DOI: https://doi.org/10.1104/pp.108.2.451, PMID: 7610156
- Suhita D, Raghavendra AS, Kwak JM, Vavasseur A. 2004. Cytoplasmic alkalization precedes reactive oxygen species production during methyl jasmonate- and abscisic acid-induced stomatal closure. *Plant Physiology* 134: 1536–1545. DOI: https://doi.org/10.1104/pp.103.032250, PMID: 15064385
- Takahashi Y, Ebisu Y, Kinoshita T, Doi M, Okuma E, Murata Y, Shimazaki K. 2013. bHLH transcription factors that facilitate K⁺ uptake during stomatal opening are repressed by abscisic acid through phosphorylation. *Science Signaling* 6:ra48. DOI: https://doi.org/10.1126/scisignal.2003760, PMID: 23779086



- Takahashi Y, Ebisu Y, Shimazaki Kl. 2017. Reconstitution of abscisic acid signaling from the receptor to DNA via bHLH transcription factors. *Plant Physiology* **174**:815–822. DOI: https://doi.org/10.1104/pp.16.01825, PMID: 28438792
- Takahashi Y, Zhang J, Hsu PK, Ceciliato PHO, Zhang L, Dubeaux G, Munemasa S, Ge C, Zhao Y, Hauser F, Schroeder JI. 2020. MAP3Kinase-dependent SnRK2-kinase activation is required for abscisic acid signal transduction and rapid osmotic stress response. *Nature Communications* 11:12. DOI: https://doi.org/10.1038/s41467-019-13875-y, PMID: 31896774
- Takahashi Y, Kinoshita T. 2015. Stomatal function has an element of hysteresis. New Phytologist 205:455–457. DOI: https://doi.org/10.1111/nph.13149, PMID: 25521066
- Ting AY, Kain KH, Klemke RL, Tsien RY. 2001. Genetically encoded fluorescent reporters of protein tyrosine kinase activities in living cells. PNAS 98:15003–15008. DOI: https://doi.org/10.1073/pnas.211564598, PMID: 11752449
- Umezawa T, Sugiyama N, Mizoguchi M, Hayashi S, Myouga F, Yamaguchi-Shinozaki K, Ishihama Y, Hirayama T, Shinozaki K. 2009. Type 2C protein phosphatases directly regulate abscisic acid-activated protein kinases in Arabidopsis. PNAS 106:17588–17593. DOI: https://doi.org/10.1073/pnas.0907095106, PMID: 19805022
- von Caemmerer S, Farquhar GD. 1981. Some relationships between the biochemistry of photosynthesis and the gas exchange of leaves. *Planta* **153**:376–387. DOI: https://doi.org/10.1007/BF00384257, PMID: 24276943
- Waadt R, Hitomi K, Nishimura N, Hitomi C, Adams SR, Getzoff ED, Schroeder JI. 2014. FRET-based reporters for the direct visualization of abscisic acid concentration changes and distribution in *Arabidopsis*. eLife 3:e01739. DOI: https://doi.org/10.7554/eLife.01739, PMID: 24737861
- Waadt R, Manalansan B, Rauniyar N, Munemasa S, Booker MA, Brandt B, Waadt C, Nusinow DA, Kay SA, Kunz HH, Schumacher K, DeLong A, Yates JR, Schroeder JI. 2015. Identification of open Stomata1-Interacting proteins reveals interactions with sucrose Non-fermenting1-Related protein Kinases2 and with type 2A protein phosphatases that function in abscisic acid responses. *Plant Physiology* **169**:760–779. DOI: https://doi.org/10.1104/pp.15.00575, PMID: 26175513
- Wang Y, Botvinick EL, Zhao Y, Berns MW, Usami S, Tsien RY, Chien S. 2005. Visualizing the mechanical activation of src. Nature 434:1040–1045. DOI: https://doi.org/10.1038/nature03469, PMID: 15846350
- Wang Y, Wang X, Gu M, Kang H, Zeng J, Fan X, Sha L, Zhang H, Yu K, Zhou Y. 2015. Cloning and characterization of four novel SnRK2 genes from *Triticum polonicum*. *Biologia Plantarum* 59:211–219. DOI: https://doi.org/10.1007/s10535-015-0501-6
- Wang P, Zhao Y, Li Z, Hsu CC, Liu X, Fu L, Hou YJ, Du Y, Xie S, Zhang C, Gao J, Cao M, Huang X, Zhu Y, Tang K, Wang X, Tao WA, Xiong Y, Zhu JK. 2018. Reciprocal regulation of the TOR kinase and ABA receptor balances plant growth and stress response. *Molecular Cell* 69:100–112. DOI: https://doi.org/10.1016/j.molcel.2017.12. 002, PMID: 29290610
- Xue S, Hu H, Ries A, Merilo E, Kollist H, Schroeder JI. 2011. Central functions of bicarbonate in S-type anion channel activation and OST1 protein kinase in CO₂ signal transduction in guard cell. *The EMBO Journal* 30: 1645–1658. DOI: https://doi.org/10.1038/emboj.2011.68, PMID: 21423149
- Yang L, Ji W, Gao P, Li Y, Cai H, Bai X, Chen Q, Zhu Y. 2012. GsAPK, an ABA-activated and calcium-independent SnRK2-type kinase from G. soja, mediates the regulation of plant tolerance to salinity and ABA stress. PLOS ONE 7:e33838. DOI: https://doi.org/10.1371/journal.pone.0033838, PMID: 22439004
- Yin Y, Adachi Y, Nakamura Y, Munemasa S, Mori IC, Murata Y. 2016. Involvement of OST1 protein kinase and PYR/PYL/RCAR receptors in methyl Jasmonate-Induced stomatal closure in *Arabidopsis* guard cells. *Plant and Cell Physiology* 57:1779–1790. DOI: https://doi.org/10.1093/pcp/pcw102, PMID: 27354421
- Yoshida R, Hobo T, Ichimura K, Mizoguchi T, Takahashi F, Aronso J, Ecker JR, Shinozaki K. 2002. ABA-activated SnRK2 protein kinase is required for dehydration stress signaling in *Arabidopsis*. *Plant and Cell Physiology* 43: 1473–1483. DOI: https://doi.org/10.1093/pcp/pcf188, PMID: 12514244
- Yoshida R, Umezawa T, Mizoguchi T, Takahashi S, Takahashi F, Shinozaki K. 2006. The regulatory domain of SRK2E/OST1/SnRK2.6 interacts with ABI1 and integrates abscisic acid (ABA) and osmotic stress signals controlling stomatal closure in *Arabidopsis. Journal of Biological Chemistry* 281:5310–5318. DOI: https://doi.org/10.1074/jbc.M509820200, PMID: 16365038
- Yoshida T, Christmann A, Yamaguchi-Shinozaki K, Grill E, Fernie AR. 2019. Revisiting the basal role of ABA Roles outside of stress. *Trends in Plant Science* 24:625–635. DOI: https://doi.org/10.1016/j.tplants.2019.04.008, PMID: 31153771
- Young JJ, Mehta S, Israelsson M, Godoski J, Grill E, Schroeder JI. 2006. CO(2) signaling in guard cells: calcium sensitivity response modulation, a ca(2+)-independent phase, and CO(2) insensitivity of the gca2 mutant. *PNAS* 103:7506–7511. DOI: https://doi.org/10.1073/pnas.0602225103, PMID: 16651523
- Zaman N, Seitz K, Kabir M, George-Schreder LS, Shepstone I, Liu Y, Zhang S, Krysan PJ. 2019. A förster resonance energy transfer sensor for live-cell imaging of mitogen-activated protein kinase activity in *Arabidopsis*. The Plant Journal **97**:970–983. DOI: https://doi.org/10.1111/tpj.14164, PMID: 30444549
- Zhang J, Ma Y, Taylor SS, Tsien RY. 2001. Genetically encoded reporters of protein kinase A activity reveal impact of substrate tethering. PNAS 98:14997–15002. DOI: https://doi.org/10.1073/pnas.211566798
- Zhang X, Henriques R, Lin SS, Niu QW, Chua NH. 2006. Agrobacterium-mediated transformation of Arabidopsis thaliana using the floral dip method. Nature Protocols 1:641–646. DOI: https://doi.org/10.1038/nprot.2006.97, PMID: 17406292
- Zhu JK. 2016. Abiotic stress signaling and responses in plants. Cell 167:313–324. DOI: https://doi.org/10.1016/j.cell.2016.08.029, PMID: 27716505



Zhu M, Geng S, Chakravorty D, Guan Q, Chen S, Assmann SM. 2020. Metabolomics of red-light-induced stomatal opening in *Arabidopsis thaliana*: coupling with abscisic acid and jasmonic acid metabolism. *The Plant Journal* **101**:1331–1348. DOI: https://doi.org/10.1111/tpj.14594, PMID: 31677315

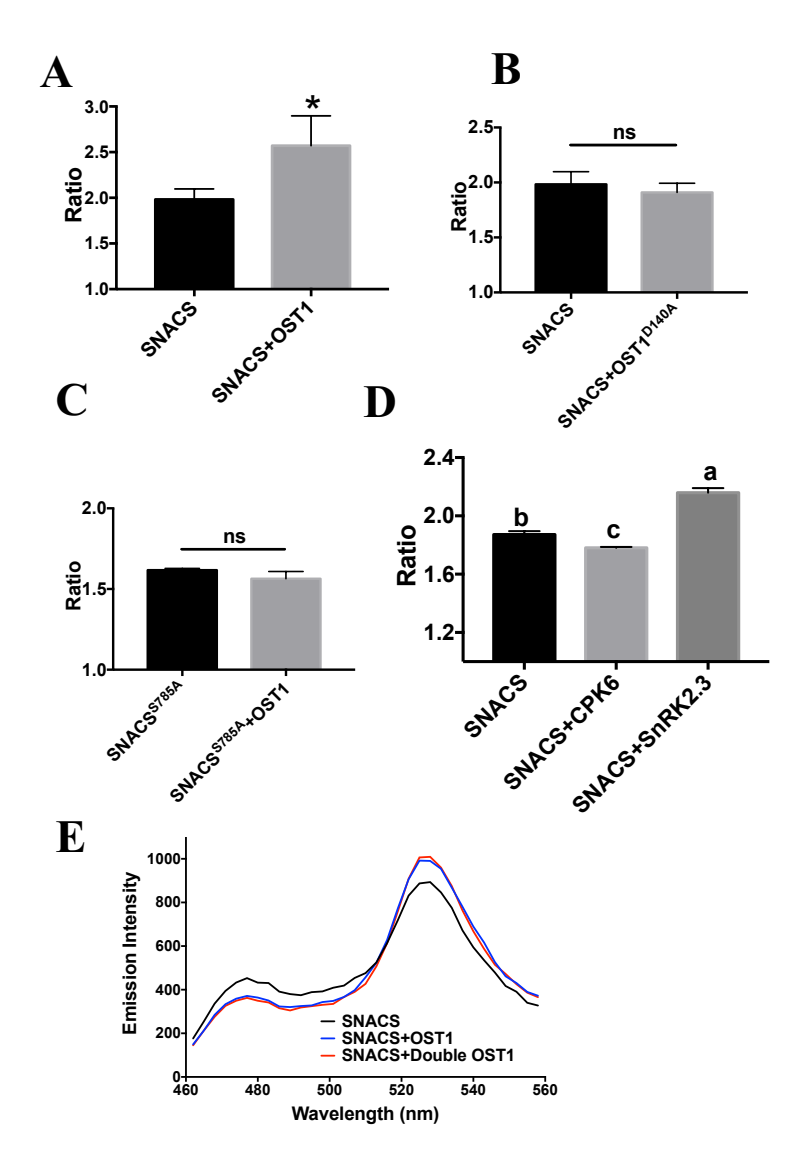


Figure 1- figure supplement 1. In vitro FRET assay of SNACS reporter

The SNACS protein or the control SNACS^{S785A} isoform was incubated *in vitro* with GST-OST1, GST-OST1^{D140A} (inactive OST1), GST-CPK6 or GST-SnRK2.3 for 2 h, respectively. The ratio was calculated from fluorescence intensities of YPet (data points, 525-531 nm) over Turquoise GL (data points, 471-477 nm).

(A) and (B) FRET ratios of *in vitro* FRET assays from three repeats using SNACS. SNACS alone controls in A and B were from the same three experiments shown in the two panels, as experiments were performed in parallel. Error bars denote mean ± SD. n=3 experiments (*P = 0.0418; ns = not significant P = 0.4214; Student's t-test).

1254 (C) In vitro FRET assays from three repeats using SNACS^{S785A}. Error bars denote mean \pm SD. n=3 1255 experiments (ns = not significant P = 0.115; Student's t-test). 1256 (D) In vitro FRET assays using SNACS with CPK6 or SnRK2.3. Means with different letters are 1257 grouped based on one-way ANOVA and Tukey's test, p<0.05 (n = 3 independent experiments). 1258 (E) In vitro FRET assays using SNACS reporter performed in the presence of two concentrations of 1259 GST-OST1 (4 µg and 8 µg). Double OST1 denotes 8 µg GST-OST1. Note that the SNACS and 1260 'SNACS+OST1' control trace in panel E is the same as the SNACS and 'SNACS+OST1' trace in 1261 Figure 1D, as these data were obtained within the same data set. 1262 1263

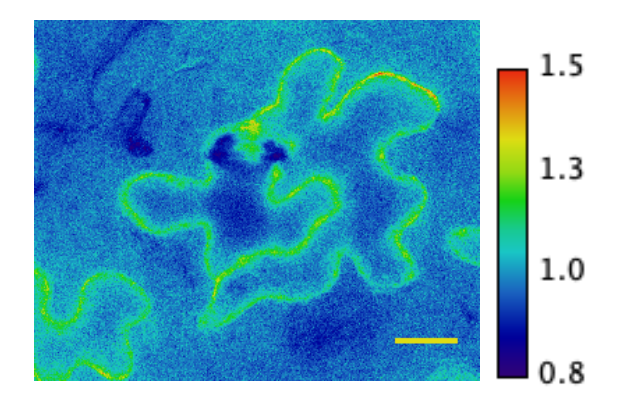


Figure 2- figure supplement 1. Ratiometric image of 535/480 nm wavelength emissions show fluorescence in SNACS-expressing *Arabidopsis* epidermal cells (pseudo-colored fluorescence ratio scale is shown on the right, non-normalized). Bar=20 μm.

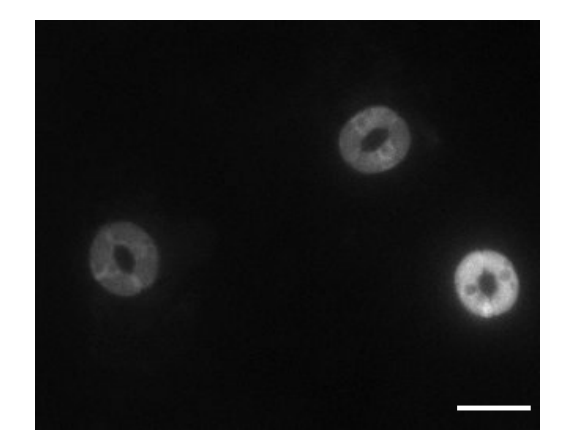


Figure 3- figure supplement 1. SNACS fluorescence appears to be observed mainly in the cytoplasm, with possible low expression in the nucleus or fluorescence may "bleed" from the cytoplasm towards the nuclear region. Stomata imaged at the SNACS YPet emission wavelength (535 nm; scale bar = $20 \mu m$).

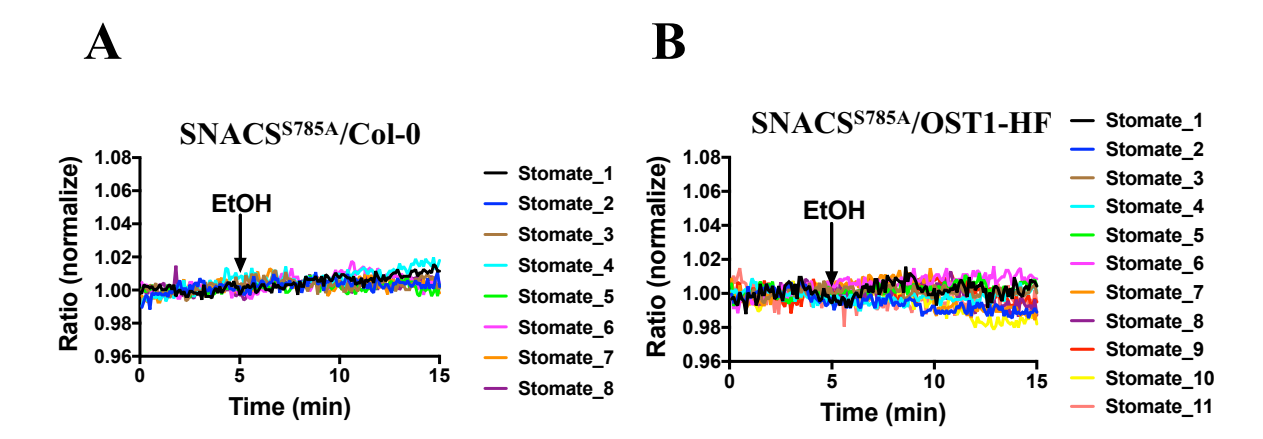


Figure 4-figure supplement 1. EtOH controls for SNACS^{S785A} in Col-0 and in *pUBQ10:OST1-HF*expressed in the *ost1-3* genetic background.

The response of the SNACS^{S785A} to EtOH (0.02%) treatment in Col-0 (A) and in *pUBQ10:OST1-HF*HF expressed in the *ost1-3* genetic background (B). The ratio of YPet to Turquoise GL emission

was normalized to the average value over the 5 minutes before treatment.

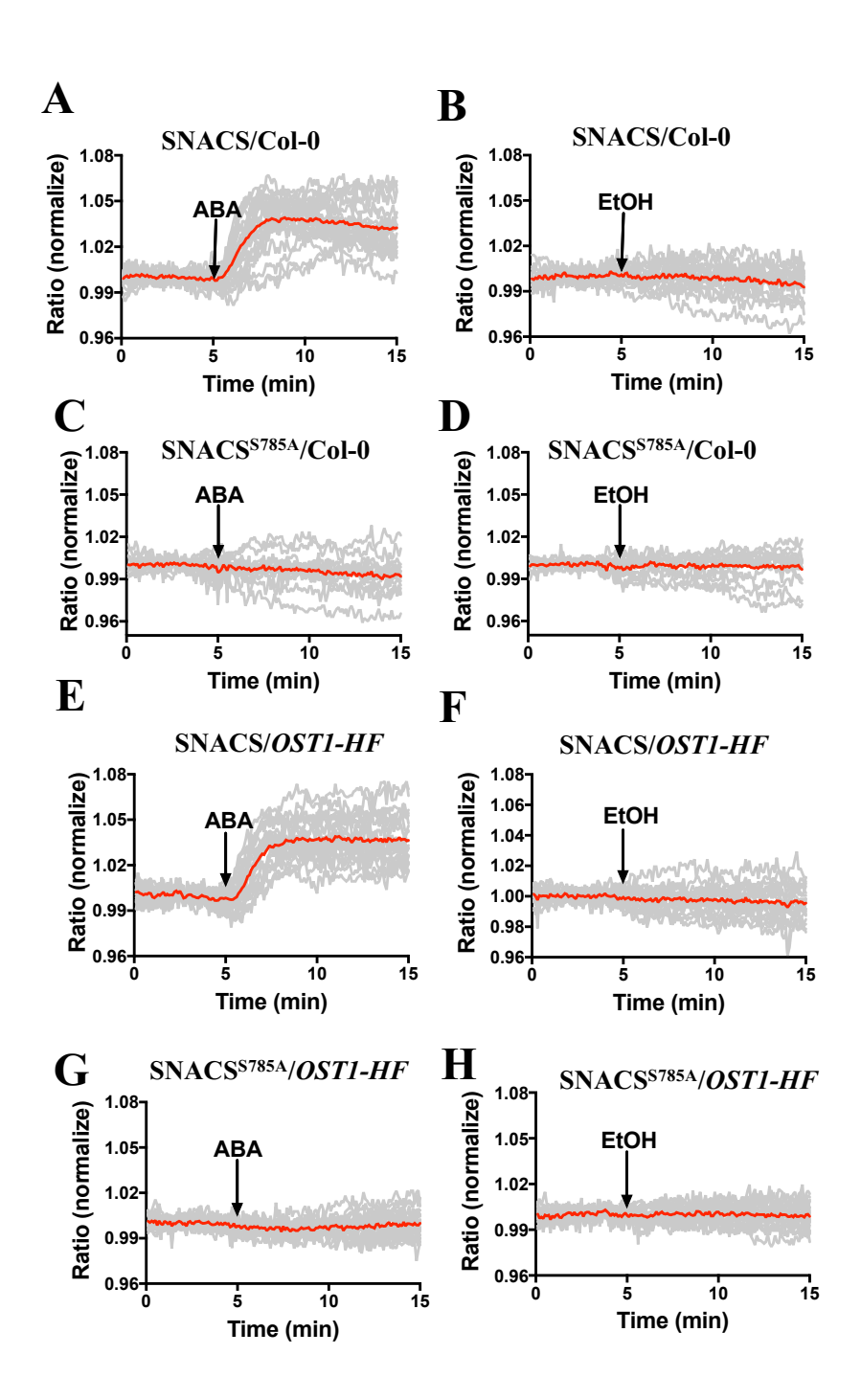


Figure 4-figure supplement 2. Combined and averages of single stomate imaging data from experimental sets including experiments in Figure 4.

Red lines show the average ratio changes of all stomata traces. Grey lines denote each single stomate ratio change. For visualization of individual stomate time courses see colored traces in Figure 4 and Figure 4-figure supplement 1. Additional data from independent experimental data sets are included

1293 in several panels of Figure 4-figure supplement 2, Figure 6-figure supplement 2, Figure 7-figure 1294 supplement 1 and Figure 8-figure supplement 1 as indicated by the total number of stomata analyzed 1295 in Supplementary Figure legends. 1296 A, B, C: data for Figure 4A-C, A: n = 24 stomata; B: n = 17 stomata, including the data shown in 1297 Figure 4B; C: n = 15 stomata, including the data shown in Figure 4C; D: data for Figure 4-figure 1298 supplement 1A, n = 13 stomata, including the data shown in Figure 4-figure supplement 1A; E, F, 1299 G: data for Figure 4E-G, n = 22 stomata, including the data shown in Figure 4E; n = 19 stomata, 1300 including the data shown in Figure 4F; n = 22 stomata, including the data shown in Figure 4G; H: 1301 data for Figure 4-figure supplement 1B, n = 19 stomata, including the data shown in Figure 4-figure 1302 supplement 1B.

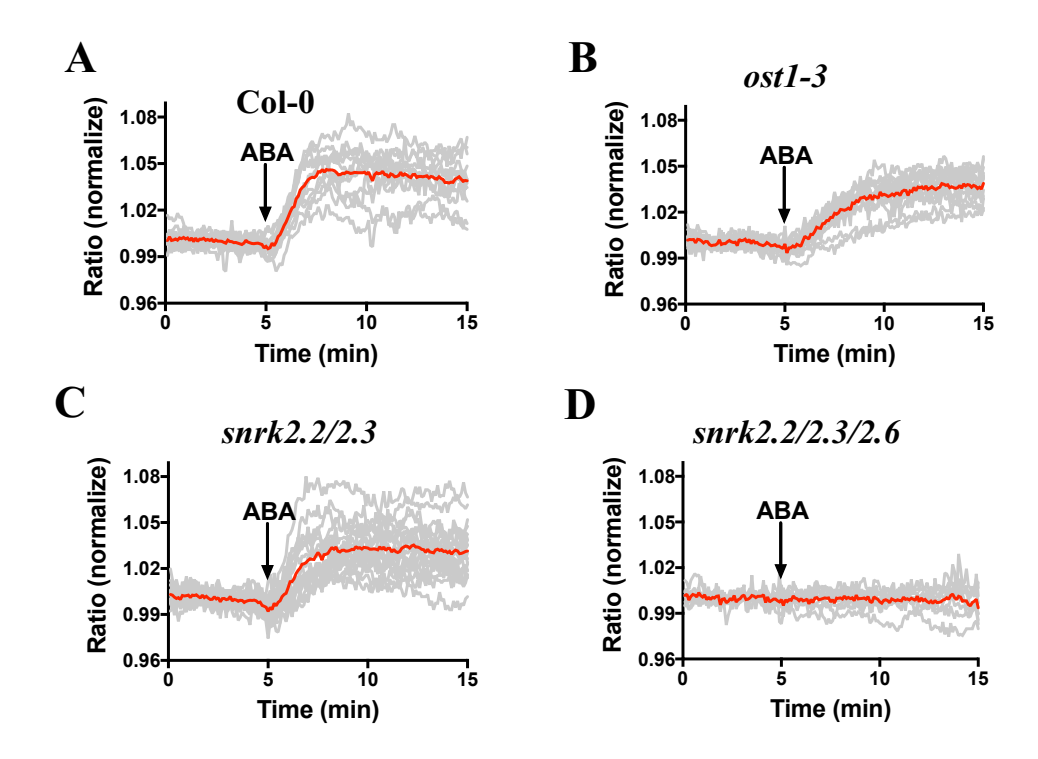


Figure 5-figure supplement 1. Combined and averages of single stomate imaging data from experimental sets shown in Figure 5.

Red lines show the average ratio changes of all stomata traces. Grey lines denote each single stomate ratio change. For visualization of individual stomate time courses see colored traces in Figure 5. A:

n = 12 stomata; B: n = 14 stomata; C: n = 20 stomata; D: n = 9 stomata.

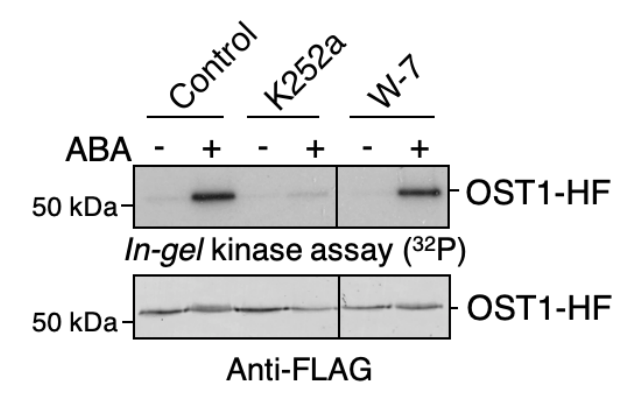


Figure 6-figure supplement 1. W-7 does not have a clear effect on ABA-induced OST1/SnRK2.6 activation in plant cells.

Mesophyll cell protoplasts prepared from stable transgenic *UBQ10:OST1-HF/ost1-3 Arabidopsis* plants were incubated with 10 μM K252a, 50 μM W-7, or DMSO (control) for 20 min. Then, protoplasts were further incubated with or without 20 μM ABA for 15 min. In-gel kinase assays show OST1/SnRK2.6 kinase activities (top panel). OST1-HF protein amounts are shown by immuno-blots using anti FLAG antibody (bottom panel).

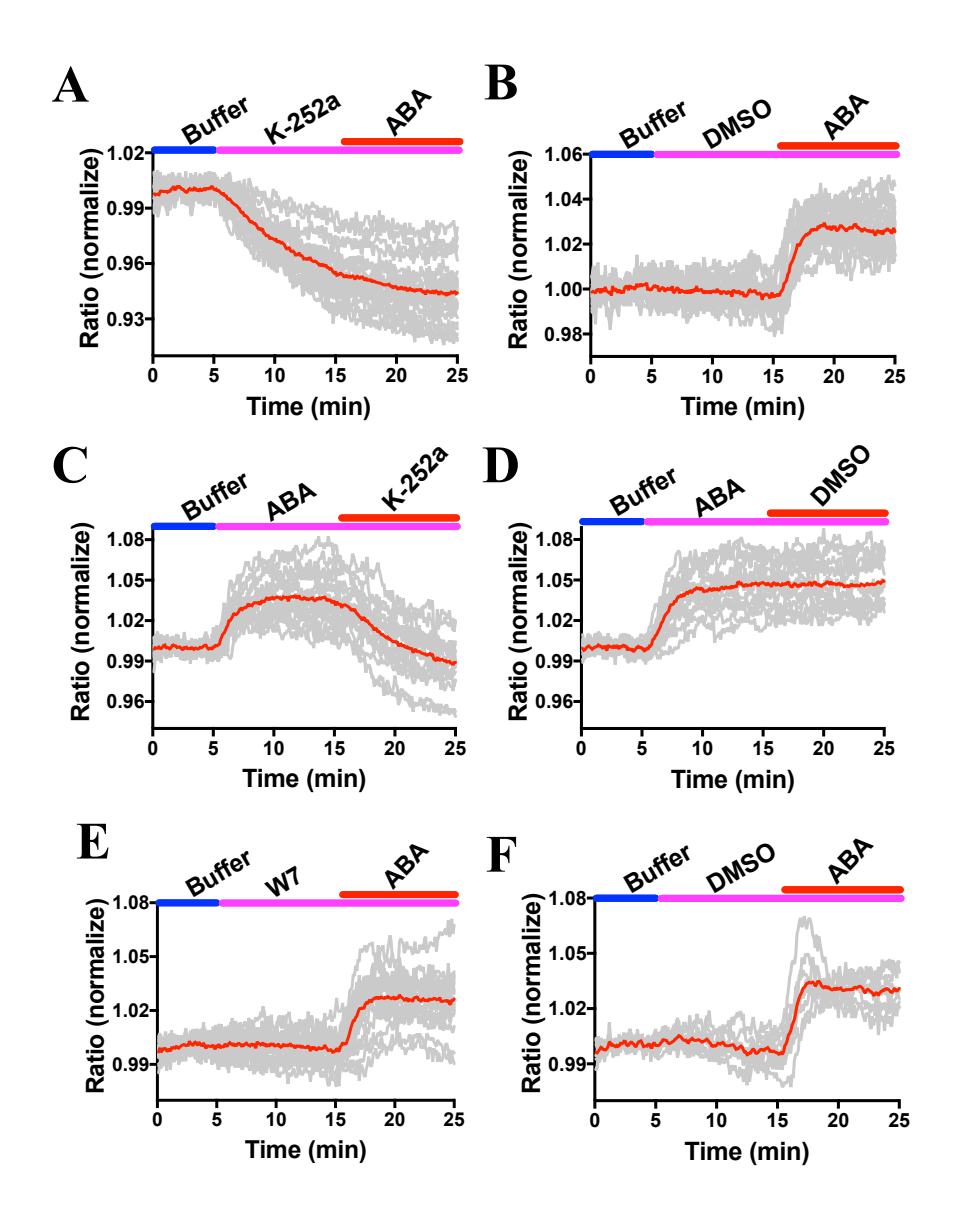


Figure 6-figure supplement 2. Combined and averages of single stomate imaging data from experimental sets including experiments in Figure 6.

Red lines show the average ratio changes of all stomata traces. Grey lines denote each single stomate ratio change. For visualization of individual stomate time courses see colored traces in Figure 6. Additional data from independent experimental data sets are included in several panels of Figure 4-figure supplement 2, Figure 6-figure supplement 2, Figure 7-figure supplement 1 and Figure 8-figure supplement 1 as indicated by the total number of stomata analyzed in Supplementary Figure

legends. A: n = 22 stomata, including the data shown in Figure 6A; B: n = 19 stomata, including the data shown in Figure 6B; C: n = 17 stomata, including the data shown in Figure 6C; D: n = 15 stomata, including the data shown in Figure 6D; E: n = 19 stomata, including the data shown in Figure 6E; F: n = 9 stomata, including the data shown in Figure 6F.

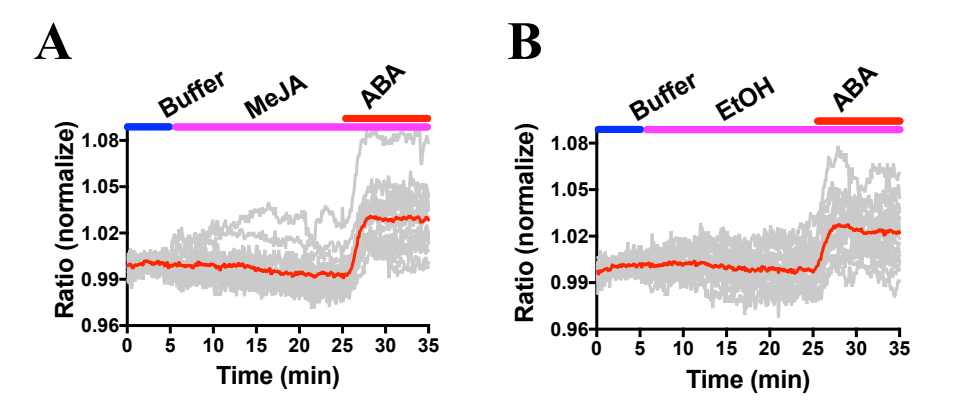


Figure 7-figure supplement 1. Combined and averages of single stomate imaging data from experimental sets including experiments in Figure 7.

Red lines show the average ratio changes of all stomata traces. Grey lines denote each single stomate ratio change. For visualization of individual stomate time courses see colored traces in Figure 7. Additional data from independent experimental data sets are included in several panels of Figure 4-figure supplement 2, Figure 6-figure supplement 2, Figure 7-figure supplement 1 and Figure 8-figure supplement 1 as indicated by the total number of stomata analyzed in Supplementary Figure legends. A: n = 18 stomata, including the data shown in Figure 7A; B: n = 18 stomata, including the data shown in Figure 7B.

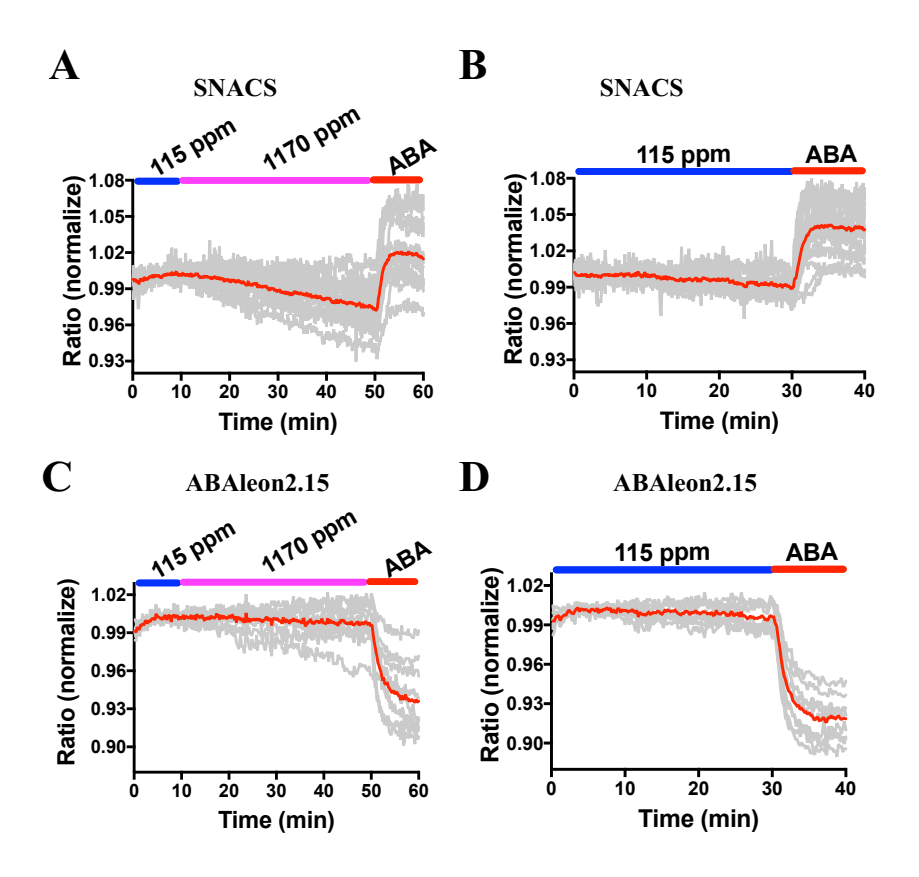


Figure 8-figure supplement 1. Combined and averages of single stomate imaging data from experimental sets including experiments in Figure 8.

Red lines show the average ratio changes of all stomata traces. Grey lines denote each single stomate ratio change. For visualization of individual stomate time courses see colored traces in Figure 8. Additional data from independent experimental data sets are included in several panels of Figure 4-figure supplement 2, Figure 6-figure supplement 2, Figure 7-figure supplement 1 and Figure 8-figure supplement 1 as indicated by the total number of stomata analyzed in Supplementary Figure legends. A: n = 15 stomata, including data shown in Figure 8A; B: n = 22 stomata, including data shown in Figure 8B; C: n = 10 stomata; D: n = 9 stomata.

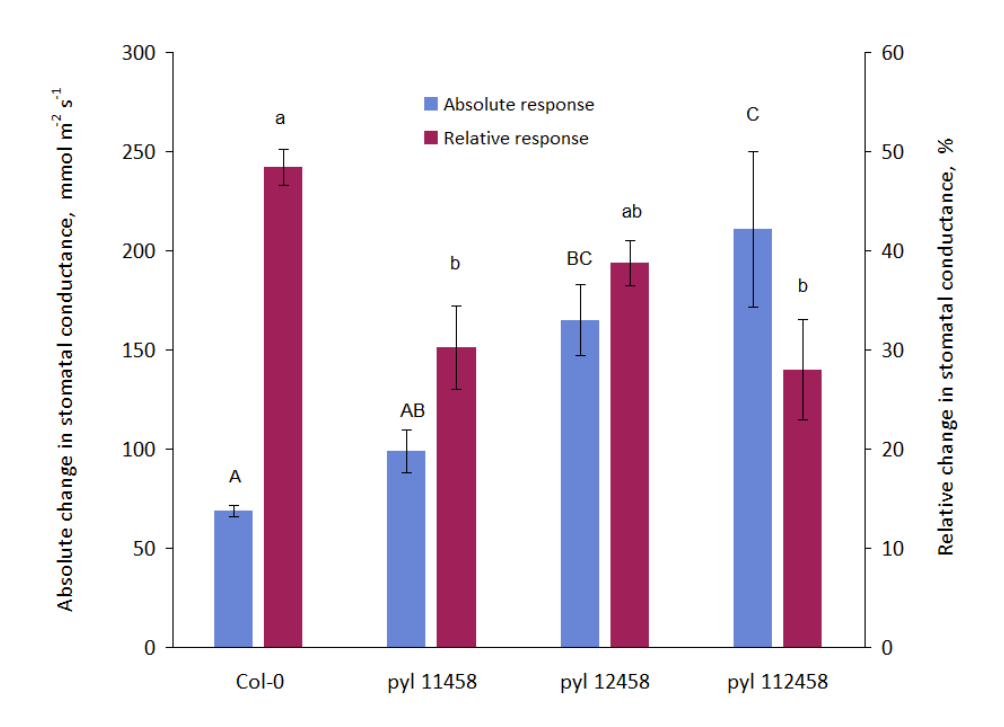
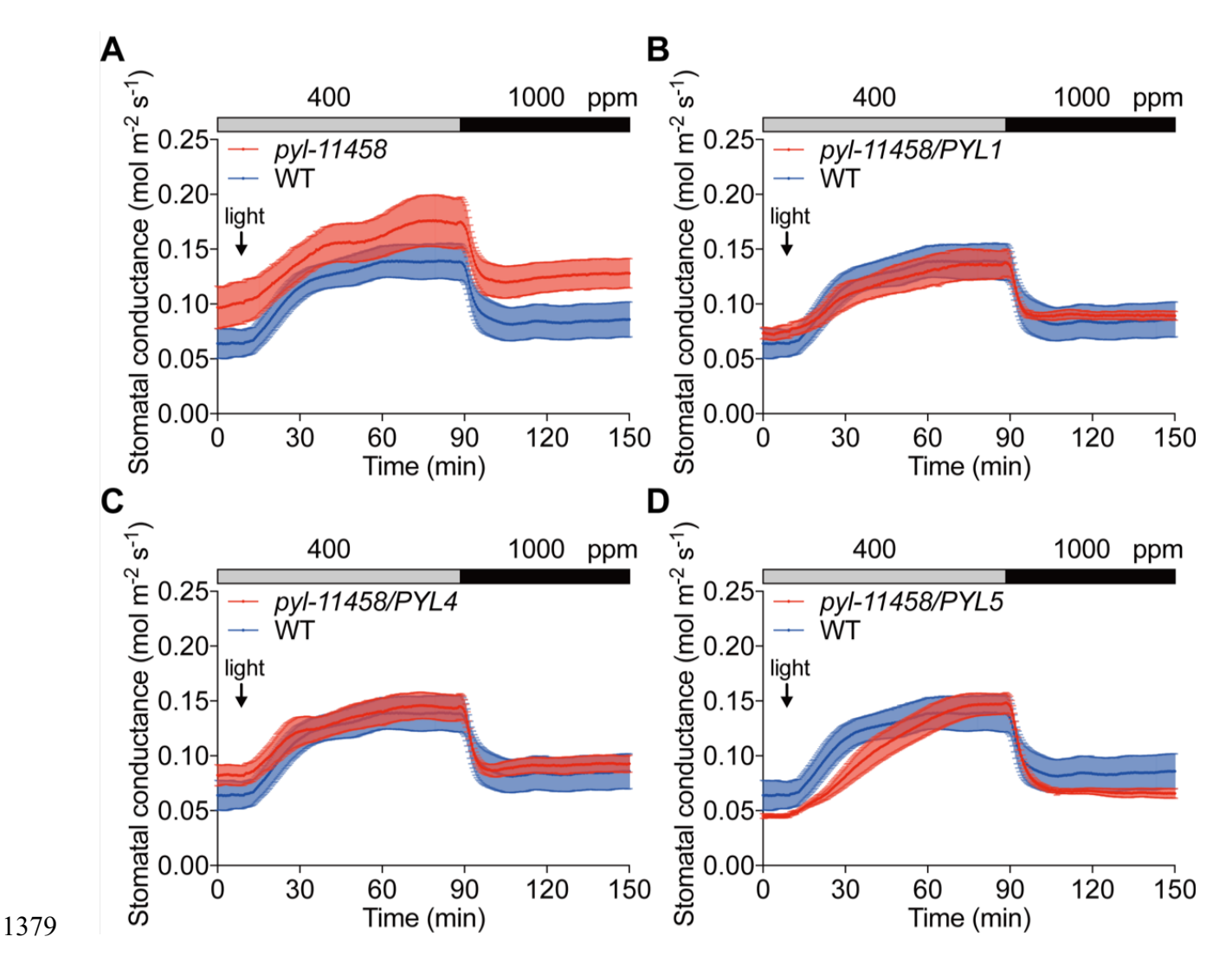


Figure 9-figure supplement 1. PYR/RCAR ABA receptor *pyr1 pyl2/4/5/8* quintuple mutant (*pyl-12458*) and *pyr1 pyl1/2/4/5/8* (*pyl-112458*) sextuple mutant show larger absolute stomatal closing responses during the first 20 minutes under elevated CO₂ compared to wild-type (Col-0) (light blue bars).

Changes in stomatal conductance (gs) after the first 20 min CO₂ elevation (gs20) in absolute units (left Y axis scale mmol m⁻² s⁻¹) and relative units (right Y axis scale in %: (gs0-gs20)/gs0). gs0 = steady state stomatal conductances prior to CO₂ elevation. In absolute units, *pyrpyl* sextuple mutant stomata close the most (light blue bars: *pyl-112458*). In contrast, in normalized units, the *pyrpyl* sextuple appears to close stomata the least compared to wild-type (dark purple bars), high-lighting pitfalls of gs normalization. Capital letters show differences in absolute responses (p=0.000158), whereas lower case letters in relative responses (p=0.00158; ANOVA, generalized linear model and Tukey post-hoc).



1381

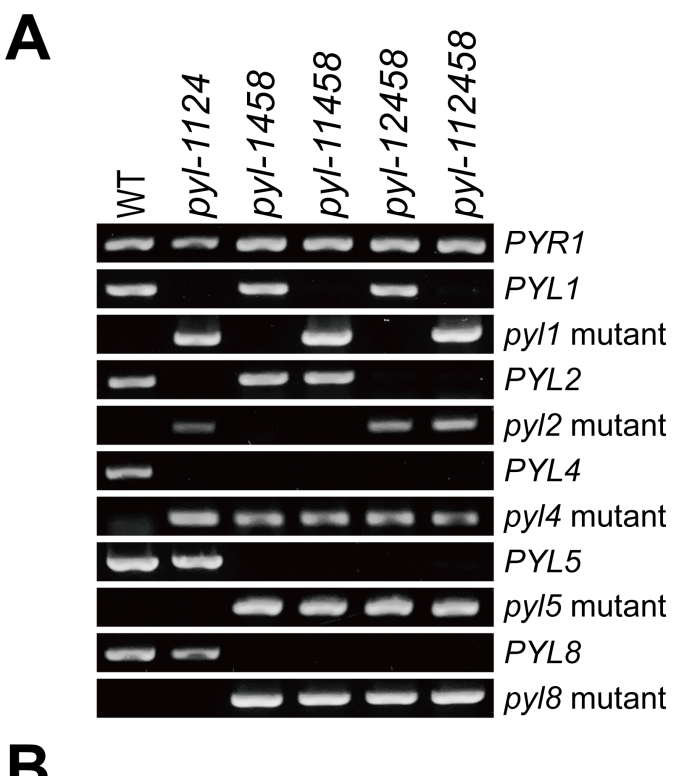
1382

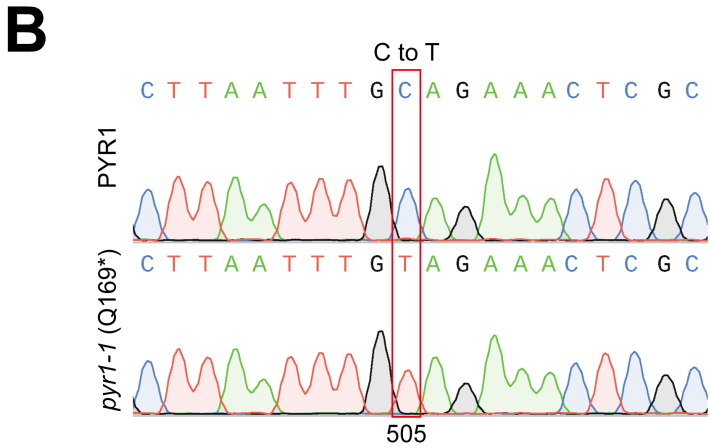
1383

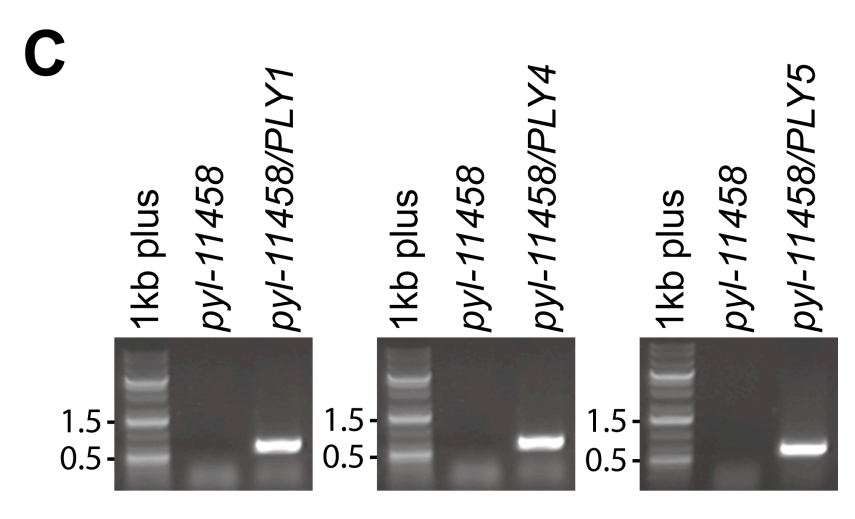
Figure 9-figure supplement 2. Stomata of ABA receptor quintuple mutant (pyr1/pyl1/pyl4/pyl5/pyl8) and guard cell-targeted (B) PYL1 and (C) PYL4 ABA receptor complemented plants show stomatal CO₂ responses similar to wild-type (Col-0) controls.

- Time-resolved stomatal conductance responses to changes in light and CO₂ concentration in Col-0
- 1385 (WT; A-D)
- 1386 (A) *pyr1/pyl1/pyl4/pyl5/pyl8* quintuple mutant (*pyl-11458*).
- 1387 (B) *pyr1/pyl1/pyl4/pyl5/pyl8/pGC1::PYL1 (pyl-11458/PYL1)*.
- 1388 (C) *pyr1/pyl1/pyl4/pyl5/pyl8/pGC1::PYL4 (pyl-11458/PYL4*).

(D) pyr1/pyl1/pyl4/pyl5/pyl8/pGC1::PYL5 (pyl-11458/PYL5). Gas exchange experiments of intact leaves commenced under dark treatment and then leaves were exposed to 125 µmol m⁻²s⁻¹ continuous light as indicated by arrow in each panel. CO₂ concentrations are shown on top of the data traces in each panel. Note that WT traces in A to D are the same for comparisons, as the indicated genotypes were measured within the same experiments. Note that steady state stomatal conductance levels in pyl-11458 mutants are conditional. Data represent mean of stomatal conductances \pm SEM. WT (n = 4), pyl-11458 quintuple (n = 4), pyl-11458/PYL1 (n = 4), pyl-11458/PYL4 (n = 5), and pyl-11458/PYL5 (n = 4).







1400 Figure 9-figure supplement 3. Genotyping of ABA receptor multiple mutants and guard cell-1401 targeted ABA receptor complemented plants. 1402 (A) Col-0 (WT) and ABA receptor higher-order mutants were confirmed by primers targeting WT 1403 or mutant alleles. Primer pairs: PYR1 (PYR1-F + PYR1-R), PYL1 (PYL1-F + PYL1-R), PYL1 1404 mutant (PYL1-F + LBb1.3), PYL2 (PYL2-F+ PYL2-R), PYL2 mutant (PYL2-F + DS5O), PYL4 1405 (PYL3-F+ PYL4-R), PYL4 mutant (PYL4-F + LB3), PYL5 (PYL5-LP+ PYL5-RP), PYL5 mutant 1406 (PYL5-RP + dSpm1), PYL8 (PYL8-F+ PYL8-R), PYL8 mutant (PYL8-F + LB3). (B) Sequence 1407 results of PYR1 in WT and pyr1-1 (Q169*) mutant allele in ABA receptor higher-order mutants. (C) 1408 Confirmation of pGC1::PYL1, pGC1::PYL4, and pGC1::PYL5 transgenes in corresponding 1409 transgenic lines, pyl-11458/PYL1, pyl-11458/PYL4, and pyl-11458/PYL5. PCR reactions were 1410 performed using pGC1-F paired with PYL1-R, PYL4-R, or PYL5-R to amplify transgenes. Primer 1411 sequences are listed in Supplementary File 2.

 Supplementary File 1. Transgenic lines used in this study.

Line name	Plasmid	Promoter	Selection	Background
SNACS/Col-0_1	35S: SNACS	CaMV 35S	Hygromycin	Col-0
SNACS/Col-0_2	35S: SNACS	CaMV 35S	Hygromycin	Col-0
SNACS ^{S785A} /Col-0_1	35S: SNACS ^{S785A}	CaMV 35S	Hygromycin	Col-0
SNACS ^{S785A} /Col-0_2	35S: SNACS ^{S785A}	CaMV 35S	Hygromycin	Col-0
SNACS/OST1-HF_1	35S: SNACS	CaMV 35S	Hygromycin	pUBQ10:OST1-HF/ost1-3
SNACS/OST1-HF_2	35S: SNACS	CaMV 35S	Hygromycin	pUBQ10:OST1-HF/ost1-3
SNACS ^{S785A} /OST1-HF_1	35S: SNACS ^{S785A}	CaMV 35S	Hygromycin	pUBQ10:OST1-HF/ost1-3
SNACS ^{S785A} /OST1-HF_2	35S: SNACS ^{S785A}	CaMV 35S	Hygromycin	pUBQ10:OST1-HF/ost1-3
SNACS/ost1-3	35S: SNACS	CaMV 35S	Hygromycin	ost1-3
SNACS/snrk2.2/2.3	35S: SNACS	CaMV 35S	Hygromycin	snrk2.2/2.3
SNACS/snrk2.2/2.3/2.6	35S: SNACS	CaMV 35S	Hygromycin	snrk2.2/2.3/2.6
pyl-11458/PYL1	pGC1: PYL1	pGC1	Seed GFP	pyr1/pyl1458
pyl-11458/PYL4	pGC1: PYL4	pGC1	Seed GFP	pyr1/pyl1458
pyl-11458/PYL5	pGC1: PYL5	pGC1	Seed GFP	pyr1/pyl1458

Supplementary File 2. Primer sequences for genotyping.

Supplemente	ary rine 20 rrimer sequences for genotyping.
Primer	Sequence
PYR1-F	ACCATGGCTTCGGAGTTAACACCA
PYR1-R	TCACGTCAC CTGAGAACCACT
PYL1-F	ATGGCGAATTCAGAGTCCTCC
PYL1-R	TTACCTAACCTGAGAAGAGTT
PYL2-F	ACCATGGGCTCATCCCCGGCCGTGA
PYL2-R	TTATTCATCATCATGCATAGGTG
PYL4-F	ACCATGGTTGCCGTTCACCGTCCTT
PYL4-R	TCACAGAGACATCTTCTTCTTGC
PYL5-LP	AAACACAAAGCCTTCACATCC
PYL5-RP	AAGTTTTGTGAATCCCCCAAC
PYL5-R	TTATTGCCGGTTGGTACTTCGA
PYL8-F	ATGGAAGCTAACGGGATTGAG
PYL8-R	TTAGACTCTCGATTCTGTCGT
LBb1.3	ATTTTGCCGATTTCGGAAC
Ds5O	GTTCGAATTCGATCGGGATAAAAC
LB3	TAGCATCTGAATTTCATAACCAATCTCGATACAC
dSpm1	CTTATTTCAGTAAGAGTGTGGGGTTTTGG
pGC1-F	CACAAGTACTATTTCACAC